Journal of Computational Physics 231 (2012) 2764–2785

Contents lists available at SciVerse ScienceDirect

Journal of Computational Physics

journal homepage: www.elsevier.com/locate/jcp

A peridynamic formulation for transient heat conduction in bodies with evolving discontinuities

Florin Bobaru [a,*], Monchai Duangpanya [b,1]

[a] Department of Mechanical and Materials Engineering, University of Nebraska-Lincoln, W307 Nebraska Hall, Lincoln, Nebraska 68588-0526, United States
[b] Chulachomklao Royal Military Academy, 26001, Thailand

ARTICLE INFO

Article history:
Received 24 July 2011
Received in revised form 27 October 2011
Accepted 15 December 2011
Available online 27 December 2011

Keywords:
Peridynamics
Nonlocal models
Heat transfer
Diffusion
Heat flux
Dynamic fracture

ABSTRACT

We introduce a multidimensional peridynamic formulation for transient heat-transfer. The model does not contain spatial derivatives and uses instead an integral over a region around a material point. By construction, the formulation converges to the classical heat transfer equations in the limit of the horizon (the nonlocal region around a point) going to zero. The new model, however, is suitable for modeling, for example, heat flow in bodies with evolving discontinuities such as growing insulated cracks. We introduce the peridynamic heat flux which exists even at sharp corners or when the isotherms are not smooth surfaces. The peridynamic heat flux coincides with the classical one in simple cases and, in general, it converges to it in the limit of the peridynamic horizon going to zero. We solve test problems and compare results with analytical solutions of the classical model or with other numerical solutions. Convergence to the classical solutions is seen in the limit of the horizon going to zero. We then solve the problem of transient heat flow in a plate in which insulated cracks grow and intersect thus changing the heat flow patterns. We also model heat transfer in a fiber-reinforced composite and observe transient but steep thermal gradients at the interfaces between the highly conductive fibers and the low conductivity matrix. Such thermal gradients can lead to delamination cracks in composites from thermal fatigue. The formulation may be used to, for example, evaluate effective thermal conductivities in bodies with an evolving distribution of insulating or permeable, possibly intersecting, cracks of arbitrary shapes.

1. Introduction and literature review

1.1. Introduction

Heat transfer problems in bodies with cracks have been studied before using the classical heat flow model. For example, Sih [1] analyzed heat transfer in an infinite plate with a crack using the complex variable theory, in a similar way as it is done in linear elastic fracture mechanics [2]. The heat-flux near the tip of an insulating crack has the same inverse square-root singularity $r^{-1/2}$ (r is the polar coordinate measured from the tip of the crack) as stresses in linear elastic fracture mechanics. Analytical results for heat flow in bodies with cracks are limited to simple geometries and boundary conditions. Heat flow in bodies with arbitrary distributions of cracks, possibly coalescing or branching, is challenging and in the literature simpler cases are treated. For example, Chen and Chang [3] used the finite element alternating method [4,5] for steady-state heat conduction problems in a plate with multiple, inclined but non-intersecting, insulated cracks. The method combines the

* Corresponding author.
E-mail address: fbobaru2@unl.edu (F. Bobaru).
[1] Lecturer.

0021-9991/$ - see front matter © 2011 Elsevier Inc. All rights reserved.
doi:10.1016/j.jcp.2011.12.017

finite element method and the Schwarz–Neumann alternating method [6]. The temperature distribution is compared with solutions for problems on an infinite strip and changing flux conditions. Chang and Ma [7] studied this problem under transient conditions. The solution in [7] is based on an iterative superposition of solutions combining the solutions for a finite plate with no cracks with those for an infinite plate with a crack.

Transient heat flow in a body with an evolving topology (such as growing cracks that may coalesce, branch, and interact, or growth of a phase with a different conductivity) is an open problem to the best of our knowledge. The formulation we propose here can solve, for the first time, such problems. Our peridynamic model for heat diffusion replaces the spatial derivatives by an integral term, which eliminates complications arising when discontinuities appear in the temperature field. Moreover, a meshfree discretization is used to numerically approximate the peridynamic equations and this allows for a simplified treatment of problems set in domains with complicated geometries or in systems with complex microstructures, which may be difficult to model with other methods.

The paper is organized as follows: after a brief motivation, we give the peridynamic formulation for heat transfer in multiple dimensions starting from ideas presented in 1D in [8]. We then define the *peridynamic heat flux* and show how to connect the micro-level peridynamic parameters to the thermal conductivity of the material. A damage model for the thermal bonds is then introduced as a means of modeling interruption of heat flow due to, for example, the presence of growing cracks, or growing insulators in the material. Details of the numerical discretization in two dimensions, including a discussion of Dirichlet and Neumann nonlocal boundary conditions, are shown in Section 3. The model is numerically tested and convergence studies in the limit of the horizon going to zero are performed in Section 4. Results are compared, in the limit of the horizon going to zero, with those from exact transient solutions of the classical model in simple geometries. In Section 5 we solve the transient heat conduction problem in a 2D plate with one or several stationary and non-intersecting cracks. We compare the results against finite element solutions (which use the classical heat equation) and other numerical solutions from the literature which also utilize the classical diffusion equation [3,7]. We then use the new formulation to solve transient heat transfer problems in bodies with evolving discontinuities, such as insulated cracks that intersect as they grow, and change the heat flow patterns, and in thermally heterogeneous material systems such as fiber-reinforced composites.

1.2. Motivation

The new peridynamic model for heat transfer proposed here may be applied to model heat transfer problems in bodies with complex, possibly evolving, thermally heterogeneous microstructure, or for simulating dynamic thermomechanical fracture and failure. Such models are important in a number of areas. For example, fracture under thermal shock is important in understanding cracking of glass used for nuclear waste vitrification [9]. Another area in which thermomechanical failure is present is the solid oxide fuel cell (SOFC). The high operating temperatures and thermal cycling in SOFCs (800–1000 °C) can induce failure through cracking [10]. Extraction of geothermal energy encounters fracturing rocks due to temperature gradients [11] and shrinkage due to cooling or drying causes cracks in basalt columns with specific spacings [12]. Dielectric breakdown of insulators [13–15], may also be modeled with the proposed peridynamic theory. Instead of having a conducting body with growing insulated cracks, in this case the body is an insulator in which conducting cracks grow and interact dynamically.

Heat transfer in biological systems (tissue, organs, etc.) and in the presence of growing tumors has become of interest recently due to, in no small measure, potential treatments of cancerous tumors using thermal ablation, via hypothermia and hyperthermia (e.g., [16–19]). The peridynamic model we introduce could be used for modeling heat transfer in such complex and thermally heterogeneous systems. Another possible application of the method introduced here is in developing peridynamic homogenized models (along the lines of [20]) for heat conduction in particle systems [21] in which loss of particle contact takes place dynamically.

2. The peridynamic formulation for multi-dimensional transient heat transfer

2.1. Derivation of the peridynamic heat transfer equation

We consider a body occupying a region Ω composed of material points that have associated mass and volume (see Fig. 1(left)). We assume thermal connections exist between each material point and neighboring points in a certain finite

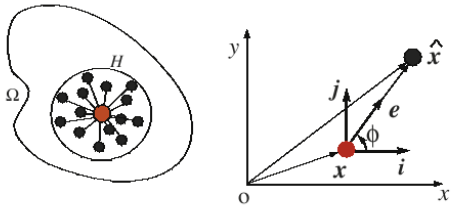

Fig. 1. The peridynamic description of a thermal body (left) and a thermal bond between $\boldsymbol{x}$ and $\hat{\boldsymbol{x}}$ (right) in 2D.

region around the point. This region is called the peridynamic horizon, H (see Fig. 1(left)). The thermal conductor between points $\boldsymbol{x}$ and $\hat{\boldsymbol{x}}$ is called a "thermal bond" or in short: t-bond (see Fig. 1(right)). For simplicity, we construct the formulation in two dimensions but the model is identical in 3D if we replace the area integral below with a volume integral. Let $\boldsymbol{i}, \boldsymbol{j}$ be unit vectors along the x-axis and y-axis respectively, and ϕ be the angle between $\boldsymbol{i}$ and the t-bond direction (see Fig. 1).

The peridynamic heat-flux corresponding to a t-bond was introduced in reference [8] as:

$$\boldsymbol{q}(\boldsymbol{x},t) = K(\boldsymbol{x},\hat{\boldsymbol{x}})\frac{\theta(\hat{\boldsymbol{x}},t)-\theta(\boldsymbol{x},t)}{\|\hat{\boldsymbol{x}}-\boldsymbol{x}\|}\boldsymbol{e} \tag{1}$$

where $K(\boldsymbol{x},\hat{\boldsymbol{x}})$ is the conductivity of the t-bond $(\boldsymbol{x},\hat{\boldsymbol{x}})$, $\theta(\hat{\boldsymbol{x}},t)-\theta(\boldsymbol{x},t)$ is the temperature difference between the two points $\boldsymbol{x}$ and $\hat{\boldsymbol{x}}$, and $\boldsymbol{e}$ is the unit vector along the t-bond $(\boldsymbol{x},\hat{\boldsymbol{x}})$.

In two dimensions, the heat transferred between $\hat{\boldsymbol{x}}$ and $\boldsymbol{x}$ along the t-bond due to their temperature difference (see Fig. 1) will generate a heat-flux vector associated with the corresponding t-bond as follows:

$$\boldsymbol{q} = K_x(\boldsymbol{x},\hat{\boldsymbol{x}})\frac{\theta(\hat{\boldsymbol{x}},t)-\theta(\boldsymbol{x},t)}{\|\hat{\boldsymbol{x}}-\boldsymbol{x}\|}\cos\phi\boldsymbol{i} + K_y(\boldsymbol{x},\hat{\boldsymbol{x}})\frac{\theta(\hat{\boldsymbol{x}},t)-\theta(\boldsymbol{x},t)}{\|\hat{\boldsymbol{x}}-\boldsymbol{x}\|}\sin\phi\boldsymbol{j} \tag{2}$$

where $K_x(\boldsymbol{x},\hat{\boldsymbol{x}})$ and $K_y(\boldsymbol{x},\hat{\boldsymbol{x}})$ are thermal conductivities of the t-bond $(\boldsymbol{x},\hat{\boldsymbol{x}})$ in x and y directions (to be related to the material conductivity), $\boldsymbol{e} = \cos\phi\boldsymbol{i} + \sin\phi\boldsymbol{j}$.

For a thermally isotropic material case, $K(\boldsymbol{x},\hat{\boldsymbol{x}}) = K_x(\boldsymbol{x},\hat{\boldsymbol{x}}) = K_y(\boldsymbol{x},\hat{\boldsymbol{x}})$. We assume that the t-bonds are insulated from each other so that there is no heat transfer along the t-bonds between them. Heat transfer happens only at the points. To use a fluid mechanics analogy, the t-bonds are like pipes transporting fluid among the "buckets" (points). The conservation of energy law led to the one-dimensional peridynamic equation for the peridynamic heat flux in a single t-bond $(\boldsymbol{x},\hat{\boldsymbol{x}})$ in the direction $\boldsymbol{e}$ (see [8]):

$$\rho c(\hat{\boldsymbol{x}}-\boldsymbol{x})\cdot\boldsymbol{e}\frac{\partial\theta_a(\boldsymbol{x},\hat{\boldsymbol{x}},t)}{\partial t} = K(\hat{\boldsymbol{x}},\boldsymbol{x})\frac{\theta(\hat{\boldsymbol{x}},t)-\theta(\boldsymbol{x},t)}{(\hat{\boldsymbol{x}}-\boldsymbol{x})\cdot\boldsymbol{e}} \tag{3}$$

where $\theta_a(\boldsymbol{x},\hat{\boldsymbol{x}},t)$ was the average temperature along the t-bond $(\boldsymbol{x},\hat{\boldsymbol{x}})$. We consider, for simplicity, that the density ρ and the specific heat c are constant. The left-hand side of Eq. (3) is the heat gain of the t-bond and the right-hand side is the heat-flux through this bond.

To obtain the peridynamic formulation for heat transfer at $\boldsymbol{x}$ due to the heat flow from all points inside its horizon (see Fig. 2), we treat $(\hat{\boldsymbol{x}}-\boldsymbol{x})\cdot\boldsymbol{e}$ or $\|\hat{\boldsymbol{x}}-\boldsymbol{x}\|$ as a finite distance, which is different from the way the energy equation is obtained in the classical heat transfer model where a limit of $\hat{\boldsymbol{x}}\to\boldsymbol{x}$ is taken. Dividing by this distance both sides of Eq. (3) and integrating over the region or the horizon, $H_{\boldsymbol{x}}$ (the disk of radius δ), we obtain:

$$\int_{H_{\boldsymbol{x}}}\rho c\frac{\partial\theta_a(\boldsymbol{x},\hat{\boldsymbol{x}},t)}{\partial t}dA_{\hat{\boldsymbol{x}}} = \int_{H_{\boldsymbol{x}}}K(\boldsymbol{x},\hat{\boldsymbol{x}})\frac{\theta(\hat{\boldsymbol{x}},t)-\theta(\boldsymbol{x},t)}{\|\hat{\boldsymbol{x}}-\boldsymbol{x}\|^2}dA_{\hat{\boldsymbol{x}}} \tag{4}$$

We assume the following connection between the temperature at $\boldsymbol{x}$ and time t and the average temperatures in all the t-bonds connected at $\boldsymbol{x}$:

$$\frac{1}{A_{\boldsymbol{x}}}\int_{H_{\boldsymbol{x}}}\rho c\theta_a(\boldsymbol{x},\hat{\boldsymbol{x}},t)dA_{\hat{\boldsymbol{x}}} = \rho c\theta(\boldsymbol{x},t)$$

where $A_{\boldsymbol{x}}$ is the area of the horizon at point $\boldsymbol{x}$. We also define the micro-conductivity of the t-bond $(\boldsymbol{x},\hat{\boldsymbol{x}})$ by

$$k(\boldsymbol{x},\hat{\boldsymbol{x}}) = K(\boldsymbol{x},\hat{\boldsymbol{x}})/A_{\boldsymbol{x}}$$

Eq. (4) then becomes:

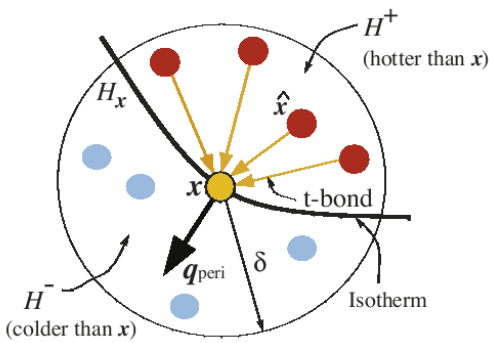

Fig. 2. The horizon, thermal bonds, and peridynamic heat flux into a point $\boldsymbol{x}$. Points located in region H^+ have higher temperatures than that of point $\boldsymbol{x}$, while points in region H^- have lower temperatures than that of $\boldsymbol{x}$. The isothermal "surface" at $\boldsymbol{x}$ does not have to be smooth, in contrast with the classical theory.

$$\rho c\frac{\partial\theta(\boldsymbol{x},\hat{\boldsymbol{x}},t)}{\partial t}=\int_{H_{\boldsymbol{x}}}k(\boldsymbol{x},\hat{\boldsymbol{x}})\frac{\theta(\hat{\boldsymbol{x}},t)-\theta(\boldsymbol{x},t)}{\|\hat{\boldsymbol{x}}-\boldsymbol{x}\|^2}dA_{\hat{\boldsymbol{x}}} \tag{5}$$

If a heat source is present at $\boldsymbol{x}$, then Eq. (5) becomes:

$$\rho c\frac{\partial\theta(\boldsymbol{x},\hat{\boldsymbol{x}},t)}{\partial t}=\int_{H_{\boldsymbol{x}}}k(\boldsymbol{x},\hat{\boldsymbol{x}})\frac{\theta(\hat{\boldsymbol{x}},t)-\theta(\boldsymbol{x},t)}{\|\hat{\boldsymbol{x}}-\boldsymbol{x}\|^2}dA_{\hat{\boldsymbol{x}}}+w(\boldsymbol{x},t) \tag{6}$$

where $w(\boldsymbol{x},t)$ is the rate of heat generation per unit area per unit time. This is the new peridynamic formulation for heat flow in 2D. For the peridynamic formulation for heat transfer in 3D one replaces the area integral with a volume integral. Note also that the formulation is consistent with the 1D formulation [8]. The Eq. (5) or (6) represent the conservation of energy (thermal energy), or the first law of thermodynamics, together with Fourier's law for heat flow, in the peridynamic formulation.

2.2. The peridynamic heat flux

In the previous section we used the notion of the peridynamic heat flux through a single t-bond. To find the peridynamic heat flux *into* a point $\boldsymbol{x}$, we consider the heat transferred to $\boldsymbol{x}$ from all points inside its horizon, that have a higher temperature than that at $\boldsymbol{x}$. We call this region H^+ (see Fig. 2). Similarly we can define the heat flux *out* of a point by considering the heat flow from the point to points within its horizon that are at a lower temperature. As a result, the new 2D peridynamics heat flux into a point $\boldsymbol{x}$ can be written as:

$$\boldsymbol{q}^{\text{peri}}(\boldsymbol{x},t)=\int_{H^+}k(\boldsymbol{x},\hat{\boldsymbol{x}})\frac{\theta(\hat{\boldsymbol{x}},t)-\theta(\boldsymbol{x},t)}{\|\hat{\boldsymbol{x}}-\boldsymbol{x}\|}\boldsymbol{e}_{\hat{\boldsymbol{x}}}dA_{\hat{\boldsymbol{x}}} \tag{7}$$

where $\boldsymbol{e}_{\hat{\boldsymbol{x}}}$ is the unit vector along the t-bond $(\boldsymbol{x},\hat{\boldsymbol{x}})$ (see Fig. 2).

We now show that, for a properly chosen micro-conductivity parameter, the peridynamic heat flux defined above is identical with the classical heat flux for a linear temperature profile. For an arbitrary temperature profile, we show that the peridynamic heat flux converges, in the limit of the horizon size δ going to zero, to the classical heat flux, for problems in domains without discontinuities.

Let us assume that the temperature varies linearly over a domain. Without loss of generality, we can assume a system of coordinates as shown in Fig. 3, aligned with the parallel isotherms.

The peridynamic heat flux vector for the configuration in Fig. 3 can be written as:

$$\begin{aligned}\boldsymbol{q}^{\text{peri}}&=\int_{H^+}k\frac{\theta(\hat{\boldsymbol{x}},t)-\theta(\boldsymbol{x},t)}{\|\hat{\boldsymbol{x}}-\boldsymbol{x}\|}\boldsymbol{e}_{\hat{\boldsymbol{x}}}dA_{\hat{\boldsymbol{x}}}=\boldsymbol{i}\int_{H^+}k\frac{\theta(\hat{\boldsymbol{x}},t)-\theta(\boldsymbol{x},t)}{\|\hat{\boldsymbol{x}}-\boldsymbol{x}\|}\cos\phi dA_{\hat{\boldsymbol{x}}}+\boldsymbol{j}\int_{H^+}k\frac{\theta(\hat{\boldsymbol{x}},t)-\theta(\boldsymbol{x},t)}{\|\hat{\boldsymbol{x}}-\boldsymbol{x}\|}\sin\phi dA_{\hat{\boldsymbol{x}}}\\&=\boldsymbol{i}\int_{H^+}k\frac{\theta(\hat{\boldsymbol{x}},t)-\theta(\boldsymbol{x},t)}{(\hat{x}-x)}\cos^2\phi dA_{\hat{\boldsymbol{x}}}+\boldsymbol{j}\int_{H^+}k\frac{\theta(\hat{\boldsymbol{x}},t)-\theta(\boldsymbol{x},t)}{(\hat{y}-y)}\sin^2\phi dA_{\hat{\boldsymbol{x}}}=\boldsymbol{i}\int_{H^+}k\frac{\theta(\hat{\boldsymbol{x}},t)-\theta(\boldsymbol{x},t)}{(\hat{x}-x)}\cos^2\phi dA_{\hat{\boldsymbol{x}}}\\&=\frac{\partial\theta(\boldsymbol{x},t)}{\partial x}\boldsymbol{i}\int_{H^+}k\cos^2\phi dA_{\hat{\boldsymbol{x}}}\end{aligned}$$

where $\boldsymbol{e}_{\hat{\boldsymbol{x}}}=\boldsymbol{i}\cos\phi+\boldsymbol{j}\sin\phi$, and $\hat{\boldsymbol{x}}-\boldsymbol{x}=(\hat{x}-x)\boldsymbol{i}+(\hat{y}-y)\boldsymbol{j}$. The integral along the $\boldsymbol{j}$ direction is zero because, for the given linear temperature profile, the integrand is an odd function integrated over a symmetrical (about the x-direction) domain.

At this point we have to introduce a connection between the micro-conductivity parameter and the material conductivity κ. We enforce that the peridynamic heat flux equals the classical heat flux for the linear temperature profile. From the above equation, the connection between k and κ, assuming a constant micro-conductivity k over the horizon is (other options are possible, see next section):

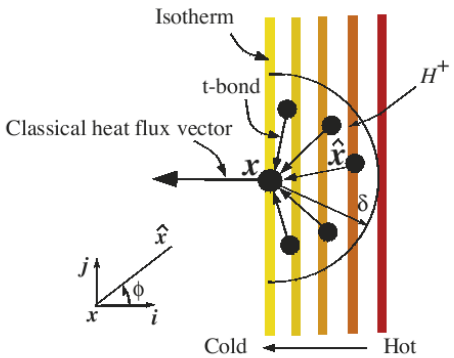

Fig. 3. A linear variation of the temperature field around point $\boldsymbol{x}$. Isotherms or isothermal surfaces are parallel lines.

$$k = \frac{\kappa}{\int_{H^+} \cos^2\phi dA_{\hat{\boldsymbol{x}}}} = \frac{4\kappa}{\pi\delta^2}.$$

The peridynamic heat flux for constant k with the above relation between the micro-conductivity of the t-bond and the thermal conductivity of the material, and for the linear temperature profile becomes:

$$\boldsymbol{q}^{\text{peri}} = \kappa \frac{\partial\theta(\boldsymbol{x},t)}{\partial x}\boldsymbol{i} = \boldsymbol{q}^{\text{classical}}$$

From the discussion above it is important to note that, for an arbitrary temperature profile the peridynamic heat flux is different from the classical one but it converges to it in the limit of the horizon going to zero and for domains without discontinuities or corners ($\boldsymbol{q}^{\text{peri}} \to \boldsymbol{q}^{\text{classical}}$ if $\delta \to 0$). It is interesting to note that while the classical heat flux is not defined at the corner of a rectangular domain, the peridynamic heat flux defined by Eq. (7) is well defined in both magnitude and direction. The same is true for the case of the heat flux at the tip of an insulating crack: the magnitude of the classical heat flux blows-up near the crack tip, whereas the peridynamic heat flux has a finite value for a given horizon size. The very general form of the peridynamic heat flux allows us to properly define a heat flux vector across surfaces that do not admit a tangent line (plane) at a point (e.g., a sharp corner, the tip of a crack, etc). In such cases, the peridynamic heat flux is no longer "normal" to the isotherm, or, alternatively, we may extend the definition of the "normal to a surface" at non-smooth points by using the proposed definition of the peridynamic heat flux.

In terms of computing the peridynamic heat flux in practice, one finds the integration region H^+ by simply comparing nodal temperatures and only adding contributions from the nodes with a temperature higher than that of the current node.

2.3. The micro-conductivity function

The micro-conductivity function plays an important role in the peridynamic model, especially at the micro-scale (the scale of the horizon), as it determines the relative thermal conductivity between points inside the horizon. At scales much larger than the horizon size, the specific shape of the micromodulus function has little influence. The shape of the micro-conductivity function also plays a role in terms of numerical approximations, as shown in, e.g., [22,23] for the micromodulus function in the mechanical peridynamic model.

Because the micro-modulus function appears under an integral sign, conditions on its smoothness are weak. In the 1D peridynamic model of heat transfer [8] the "constant" and the "triangular" micro-conductivity functions were used. Here we extend these to the 2D case.

In principle, it should be possible to obtain a physically-based specific profile of the micro-conductivity function for a particular material (from micro-scale heat conduction experiments, for example). In what follows we determine the micro-conductivity functions in terms of the material conductivity by enforcing a match between the peridynamic heat flux and the classical heat flux values generated by a linear temperature profile, under steady-state conditions.

Assume a temperature distribution of the following form: $\theta(x,y,t) = ax + b$ where a, b are constants (see Fig. 3). To find the relation between the material thermal conductivity $\kappa$and micro-conductivity $k(\hat{\boldsymbol{x}},\boldsymbol{x})$ of the t-bonds, we enforce a match between the classical heat flux at point $\boldsymbol{x}$ across the isotherm surface (see Fig. 3) and the peridynamic heat flux:

$$q^{\text{classical}}(\boldsymbol{x}) = \kappa\frac{\partial\theta(x,y)}{\partial x} = \kappa a \equiv q^{\text{peri}}(\boldsymbol{x}) = \int_{-\pi/2}^{\pi/2}\int_0^{\delta} k(\boldsymbol{x},\hat{\boldsymbol{x}})\frac{\theta(\hat{\boldsymbol{x}})-\theta(\boldsymbol{x})}{(\hat{x}-x)}\cos^2\phi r\, dr d\phi = \int_{-\pi/2}^{\pi/2}\int_0^{\delta} ak(\boldsymbol{x},\hat{\boldsymbol{x}})\cos^2\phi r\, dr d\phi$$

where $\boldsymbol{x} = \boldsymbol{x}(x,y), \hat{\boldsymbol{x}} = \hat{\boldsymbol{x}}(\hat{x},\hat{y})$ and $\cos\phi = \frac{(\hat{x}-x)}{\|\hat{\boldsymbol{x}}-\boldsymbol{x}\|}$.

Remark 1. $\|\hat{\boldsymbol{x}}-\boldsymbol{x}\|$ is the Euclidean distance between $\hat{\boldsymbol{x}}$ and x, while $(\hat{x}-x)$ is the distance in the x-direction between $\hat{\boldsymbol{x}}$ and x.

2.3.1. The constant micro-conductivity function

The constant function is defined as (see Fig. 4(left)):

$$k(\boldsymbol{x},\hat{\boldsymbol{x}}) = k_0$$

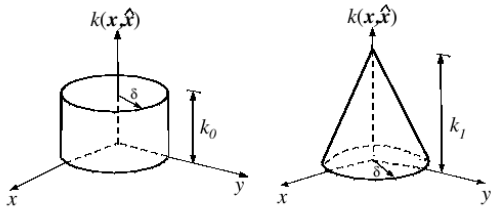

Fig. 4. The constant (left) and conical (right) micro-conductivity functions.

The constant k_0 was obtained before when we showed the identity between the peridynamic heat flux and the classical heat flux. Here again, from above, the peridynamic heat flux at $\boldsymbol{x}$ is:

$$q^{\text{peri}}(\boldsymbol{x}) = \int_{-\pi/2}^{\pi/2} \int_0^{\delta} k_0 \frac{\theta(\hat{\boldsymbol{x}}) - \theta(\boldsymbol{x})}{(\hat{x} - x)} \cos^2\phi r dr d\phi = k_0 a \pi \delta^2 / 4$$

which leads to

$$k_0 = \frac{4\kappa}{\pi\delta^2}.$$

2.3.2. The conical micro-conductivity function

The simplest micro-conductivity function that depends on the relative distance between the material points is the conical micro-conductivity function defined as (see Fig. 4(right)):

$$k(\boldsymbol{x}, \hat{\boldsymbol{x}}) = k_1\left(1 - \frac{r}{\delta}\right)$$

where $r = \|\hat{\boldsymbol{x}} - \boldsymbol{x}\|$. The peridynamic heat flux at $\boldsymbol{x}$ is:

$$q_x^{\text{peri}} = \int_{-\pi/2}^{\pi/2} \int_0^{\delta} k_1\left(1 - \frac{r}{\delta}\right) \frac{\theta(\hat{\boldsymbol{x}}) - \theta(\boldsymbol{x})}{(\hat{x} - x)} \cos^2\phi r \, dr d\phi = k_1 \delta^2 \frac{a\pi}{12}$$

and this leads to:

$$k_1 = \frac{12\kappa}{\pi\delta^2}\left(1 - \frac{r}{\delta}\right).$$

Remark 2. As discussed above, the specific profile of the micro-conductivity function is irrelevant at scales much larger than the horizon scale. Note that, for example, in thermally heterogeneous materials, the specific shape and size of the inclusions will define a certain material length-scale that is relevant at the macro scale. In an explicit model of the inclusions, the horizon size needs to be sufficiently smaller than the inclusions' length-scale (see Fig. 5) in order for the peridynamic equations to give results that are insensitive to the specific profile of the micro-conductivity function. For these kinds of heterogeneous problems, the shape and size of the inclusions gives guidance on the appropriate horizon size. Obviously, in a homogenized model of the heterogeneous material, the specific shape of the micro-conductivity function is irrelevant if the horizon is much smaller than the geometrical features of the system under investigation. This will become clearer through the numerical examples and convergence studies below.

2.4. A thermal material with damage

Damage of thermal bonds can be caused by a variety of reasons. A common situation is the emergence of cracks or of growing of an insulator or of a phase with a different thermal conductivity in the material. Heat conduction across insulated cracks is suppressed, and across cracks in general is affected. We choose to link damage of thermal bonds to the mechanical failure of the mechanical peridynamic bonds. Damage of bonds in peridynamics has been introduced in [24]. Damage of bonds in the peridynamic formulation of heat diffusion has been originally introduced in [8]. In this section we extend that formulation to the multi-dimensional case and also generalize it to cover partial damage of the thermal bonds that can model cases when heat conduction is only partially interrupted when the mechanical bonds break. An example is the case of a crack that propagates but then closes and heat conduction resumes but only partially.

First, let us denote the kernel function in Eq. (5) as follows:

$$\rho c \frac{\partial\theta(\boldsymbol{x}, \hat{\boldsymbol{x}}, t)}{\partial t} = \int_{H_x} k(\boldsymbol{x}, \hat{\boldsymbol{x}}) \frac{\theta(\hat{\boldsymbol{x}}, t) - \theta(\boldsymbol{x}, t)}{\|\hat{\boldsymbol{x}} - \boldsymbol{x}\|^2} dA_{\hat{\boldsymbol{x}}} = \int_{H_x} \Theta(\boldsymbol{x}, \hat{\boldsymbol{x}}, \theta(\boldsymbol{x}, t), \theta(\hat{\boldsymbol{x}}, t), t) d\hat{\boldsymbol{x}} \tag{8}$$

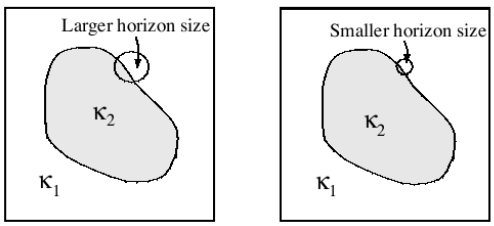

Fig. 5. In an explicit model of thermally heterogeneous inclusions, the horizon size needs to be significantly smaller than the inclusion scale in order to obtain peridynamic results insensitive to the particular profile of the micro-conductivity function.

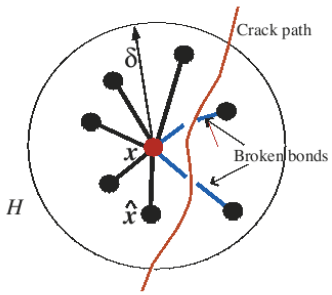

Fig. 6. Mechanically broken bonds can interrupt, or more generally affect, heat flow. In this case, the peridynamic bonds are thermo-mechanical bonds.

where Θ is a scalar-valued function. To model a thermal material with damage, the function Θ in Eq. (8) is set to be a "*history-dependent*" function:

$$\widetilde{\Theta}(\boldsymbol{x},\hat{\boldsymbol{x}},\theta(\boldsymbol{x},t),\theta(\hat{\boldsymbol{x}},t),t)=\Theta(\boldsymbol{x},\hat{\boldsymbol{x}},\theta(\boldsymbol{x},t),\theta(\hat{\boldsymbol{x}},t),t)\mu(t,\|\hat{\boldsymbol{x}}-\boldsymbol{x}\|) \tag{9}$$

where μ is a history-dependent scalar-valued function defined by

$$\mu(t,\|\hat{\boldsymbol{x}}-\boldsymbol{x}\|)=\begin{cases}1, & \text{if} \quad e(\tau,\xi,\boldsymbol{\eta})<e_0 \quad \text{for all} \quad 0\leqslant\tau\leqslant t\\ \alpha(\tau,\xi,\boldsymbol{\eta}), & \text{otherwise}\end{cases} \tag{10}$$

Here,

$$e=\frac{\|\xi+\boldsymbol{\eta}\|-\|\xi\|}{\|\xi\|} \tag{11}$$

is the "*relative elongation*" of a bond, e_0 is the critical relative elongation of the bond, $\xi=\hat{\boldsymbol{x}}-\boldsymbol{x}$ is the relative position vector in the initial configuration and $\boldsymbol{\eta}=\boldsymbol{u}(\hat{\boldsymbol{x}},t)-\boldsymbol{u}(\boldsymbol{x},t)$ is the relative displacement vector (see, e.g., [23,25]). The scalar-valued function α is zero if the crack can be assimilated with an insulated crack, and is a sub-unitary number if conduction is only partially reduced by the crack formed.

The function α above can also be used to model heat transfer through convection or radiation processes. This topic is not considered here. In Fig. 6 we show a situation in which some of the bonds are broken. In computations, a measure for the amount of damage at a point is defined by the ratio between the number of broken bonds and the number of original bonds [24].

3. Numerical discretization in 2D

We use a uniform grid, with grid spacing Δx, to discretize the domain for two dimensional heat conduction because these types of grids are the easiest to generate and work with. All points or nodes have their own area (or volume in 3D) (see Fig. 7). The area of a node in the bulk is therefore $A=(\Delta x)^2$, nodes at a 90° corner of the domain have areas equal to $A/4$, and those on a flat boundary $A/2$. A discretization in which all nodes have the same area associated with them is also possible and this was done in the 1D paper [8], but in this case if we want nodes to be located on the boundary of the domain, there will be a certain peridynamic "skin" area outside of the exact geometry. Except for scales in the order of the horizon size, results with both types of approaches are basically the same, for sufficiently fine discretizations (see also the discussion in [8]). In all examples below we use the approach with nodes having "partial areas" at the edges of the domain. A mid-point numerical integration is used to approximate temperature and heat flux distributions. While this is reasonable for nodes in the bulk, for nodes on the boundary, which are not placed at the centroid of their areas, this will result in some larger numerical integration error. The error should subside once the ratio of the horizon to the grid spacing increases. This topic is discussed in more detail in Section 4.1.2.

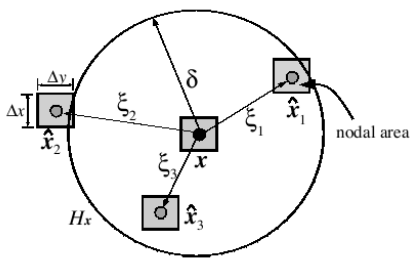

Fig. 7. Areas of nodes $\hat{\boldsymbol{x}}$ covered by the horizon of $\boldsymbol{x}$. ξ is the distance $\|\hat{\boldsymbol{x}}-\boldsymbol{x}\|$.

As a result of the spatial discretization, the peridynamic heat equation at a node $\boldsymbol{x}_i$ (from Eq. (5)) is:

$$\rho c\dot{\theta}(\boldsymbol{x}_i,t)=\sum_p k(\boldsymbol{x}_i,\boldsymbol{x}_p)\frac{\theta(\boldsymbol{x}_p,t)-\theta(\boldsymbol{x}_i,t)}{r_{ip}^2}A_{ip} \tag{12}$$

where the summation includes all nodes $\boldsymbol{x}_p$'s located inside the horizon of node $\boldsymbol{x}_i$. A_{ip} is the area of node $\boldsymbol{x}_p$ covered by the horizon of node $\boldsymbol{x}_i$. r_{ip} is the distance between nodes $\boldsymbol{x}_i$ and $\boldsymbol{x}_p$.

Note that in the above approximation, the term for $p = i$ is indeterminate (zero divided by zero case). The actual value for this term, however, exists, and physically it represents the amount of heat stored in the area of node $\boldsymbol{x}_i$. Analytically this can be computed using a limit process. Here we use the following average from the eight nodes surrounding $\boldsymbol{x}_i$ to approximate it:

$$\frac{1}{8}\sum_{j=1}^{8} k(\boldsymbol{x}_k,\boldsymbol{x}_i)\frac{\theta(\boldsymbol{x}_k,t)-\theta(\boldsymbol{x}_i,t)}{s_{ik}^2}A_i$$

where $s_{ik}=\frac{r_{ik}}{2}$ and A_i is the area of node $\boldsymbol{x}_i$.

For time integration we use the fourth-order Runge–Kutta method. A stable time step $t = 10^{-6}$ s (determined using the formula obtained in [24]) is used in all tests.

3.1. Imposing the nonlocal Dirichlet (temperature) boundary conditions

For simplicity and consistency with the way Dirichlet boundary conditions are imposed in numerical methods that discretize the classical, local, model of heat transfer, we choose to apply the nonlocal Dirichlet boundary conditions directly at the boundary nodes only. In principle, since the peridynamic formulation is nonlocal, such boundary conditions are imposed over a layer of thickness δ, the peridynamic horizon, inside the surface of the body (see [26]). Numerical tests have shown that these two versions are equivalent means of imposing such boundary conditions, in the sense that away from the Dirichlet portion of the boundary, the solutions are identical. In the numerical examples given in this work we simply assign the given temperature value to all nodes on the boundaries where Dirichlet conditions are imposed.

3.2. Imposing nonlocal Neumann (heat flux) boundary conditions

We here discuss only the case of constant heat flux imposed on a boundary. This can be easily modified to implement more general cases in which the heat-flux varies. To impose a constant heat flux, of magnitude q_x in the x-direction at nodes along a flux boundary, we follow the procedure developed previously for the 1D case (see [8]) and find the relationship between the temperature values at the boundary node $\boldsymbol{x}_i$ and the nodes located inside the horizon of this boundary node, so that the resulting classical heat-flux is the same as the imposed value q_x. From Section 2.2, the heat flux into point $\boldsymbol{x}$ in the x-direction is:

$$q_x^{\text{peri}}(\boldsymbol{x},t)=\int_{H^+} k\frac{\theta(\hat{\boldsymbol{x}},t)-\theta(\boldsymbol{x},t)}{\|\hat{\boldsymbol{x}}-\boldsymbol{x}\|}\cos\phi dA_{\hat{\boldsymbol{x}}}$$

Using the mid-point numerical integration the peridynamic heat flux at a node $\boldsymbol{x}_i$ in x-direction is approximated by

$$\begin{aligned} q_x^{\text{peri}}(\boldsymbol{x},t) &\approx \sum_p k(\boldsymbol{x}_i,\boldsymbol{x}_p)\frac{\theta(\boldsymbol{x}_p,t)-\theta(\boldsymbol{x}_i,t)}{r_{ip}}\cos\phi A_{ip}=\sum_p k(\boldsymbol{x}_i,\boldsymbol{x}_p)\frac{\theta(\boldsymbol{x}_p,t)-\theta(\boldsymbol{x}_i,t)}{r_{ip}^2}L_{ip}^x A_{ip}\\ &=\sum_p k(\boldsymbol{x}_i,\boldsymbol{x}_p)\frac{\theta(\boldsymbol{x}_p,t)}{r_{ip}^2}L_{ip}^x A_{ip}-\theta(\boldsymbol{x}_i,t)\sum_p k(\boldsymbol{x}_i,\boldsymbol{x}_p)\frac{L_{ip}^x A_{ip}}{r_{ip}^2} \end{aligned}$$

where $L_{ip}^x=x_p-x_i, r_{ip}=\|\boldsymbol{x}_p-\boldsymbol{x}_i\|$, and $\cos\phi=L_{ip}^x/r_{ip}$. Solving for the temperature at $\boldsymbol{x}_i$ in terms of the temperatures of nodes in its horizon, and imposing that the peridynamic heat flux matches the given value q_x, we obtain:

$$\theta(\boldsymbol{x}_i,t)=\frac{\sum_p k(\boldsymbol{x}_i,\boldsymbol{x}_p)\theta(\boldsymbol{x}_p,t)L_{ip}^x A_{ip}/r_{ip}^2-q_x}{\sum_p k(\boldsymbol{x}_i,\boldsymbol{x}_p)L_{ip}^x A_{ip}/r_{ip}^2}$$

Similarly, to impose a heat-flux of magnitude q_y in the y-direction at a boundary node, $\boldsymbol{x}_i$, the relationship that needs to be enforced is:

$$\theta(\boldsymbol{x}_i,t)=\frac{\sum_p k(\boldsymbol{x}_i,\boldsymbol{x}_p)\theta(\boldsymbol{x}_p,t)L_{ip}^y A_{ip}/r_{ip}^2-q_y}{\sum_p k(\boldsymbol{x}_i,\boldsymbol{x}_p)L_{ip}^y A_{ip}/r_{ip}^2}$$

Note that in the 1D case (see [8]) it is easy to specify temperatures for all nodes inside the horizon of a boundary node so that the imposed value of the heat flux is obtained. In higher dimensions, such relationships are more difficult to derive and implement and the advantages, compared to the above scheme in which we only specify the temperature at the boundary nodes only, are minor.

Note also that as the horizon goes to zero and the peridynamic heat flux converges to the classical heat flux, the approach presented above leads an exact imposition of the given heat flux.

3.3. Calculating the area of a node covered by the horizon of a given node

As seen from Eq. (12), the discrete version of the peridynamic equations obtained using the composite mid-point integration scheme requires the computation of the area (or volume in 3D) of node $\boldsymbol{x}_p$ covered by the horizon of node $\boldsymbol{x}_i$, A_{ip}. Exact calculation of this is not easy to perform for nodes that are not entirely contained inside the horizon of node $\boldsymbol{x}_i$. Here we employ an approximation originally proposed in [27]. Simpler algorithms than the one introduced in [27] can be used, with the simplest being based on the relative distance between nodes $\boldsymbol{x}_i$ and $\boldsymbol{x}_p$: if the distance is less than δ then the entire nodal area of $\boldsymbol{x}_p$ is considered inside the horizon, and if the distance is larger than δ then the "inside" area is taken to be zero. Such an algorithm, however, leads to non-uniform m-convergence results (see [27]) and also to non-uniformities along different radial directions drawn from the node $\boldsymbol{x}_i$. The algorithm below leads to a more uniform behavior for this numerical integration scheme. For the conical micromodulus, the algorithm also adjusts the value of the relative distance between nodes for nodes near the boundary (see [27]). The algorithm below is for a uniform grid, with $\Delta x = \Delta y$ (see Fig. 7) and the conical micromodulus function.

Algorithm 1: Calculating the area A_{ip} of a node $\boldsymbol{x}_p$ covered by the horizon of a given node $\boldsymbol{x}_i$ for the conical micromodulus function (from [27])

Require: $\Delta x = \Delta y$
1: **if** $\xi_{ip} < \delta - \frac{\Delta x}{2}$ **then**
2: factor = 1
3: Evaluate micro-conductivity k at $\xi_{ip} = \|\boldsymbol{x}_i - \boldsymbol{x}_p\|$
4: **else if** $\xi_{ip} \leqslant \delta$ **then**
5: factor = $(\delta + \Delta x/2 - \xi_{ip})/\Delta x$
6: Evaluate micro-conductivity k at $\xi = \xi_{ip} - \Delta x * (1 - \text{factor})/2$
7: **else if** $\xi_{ip} \leqslant \delta + \Delta x/2$ **then**
8: factor = $(\delta + \Delta x/2 - \xi_{ip})/\Delta x$
9: Evaluate micro-conductivity k at $\xi = \delta - \Delta x * \text{factor}/2$
10: **else**
11: factor = 0
12: **end if**
13: $A_{ip} = \text{factor} * (\Delta x)^2$

3.4. Finding broken t-bonds for pre-cracks

If there are initial cracks or "needle"-like thermally heterogeneous inclusions in the thermal body we need to determine the thermal bonds that cross such features and assign them different micro-conductivity properties, such as zero conductivity for the case of t-bonds crossing an insulating crack. Assume that an initial insulating crack is defined by the segment ***CD*** and assume a t-bond is defined by the segment ***AB***. If this t-bond crosses the crack, heat transfer through it is interrupted. The test for the crossing of the two segments is:

- if $(\boldsymbol{AC} \times \boldsymbol{AB}) \cdot (\boldsymbol{AD} \times \boldsymbol{AB}) < 0$, and
- if $(\boldsymbol{CA} \times \boldsymbol{CD}) \cdot (\boldsymbol{CB} \times \boldsymbol{CD}) < 0$ then the t-bond ***AB*** crosses the crack segment ***CD***.

3.5. Calculating the peridynamic temperature and heat flux near an insulating crack

Near a domain boundary or close to an insulating crack, the peridynamic horizon is not a full disk (see Fig. 6). The computation of the micro-conductivity parameter was performed assuming integration over a full horizon. In principle, in order to match the same bulk-material conductivity parameter while integrating over a smaller area (due to the presence of a boundary or of an insulating crack) one has to increase the value of the t-bond micro-conductivity to compensate for the loss of integration area. For the mechanical peridynamic formulation, these issues are discussed in [25] not only in terms of the micro-modulus of the bonds but also in terms of the critical relative elongation of the bonds (which is connected to the energy release rate of the material) and their dependence on existing damage in the material. While such modification can be made in the thermal case so that the micro-conductivity depends on the number of "missing" t-bonds for a node near a crack, in this paper we choose not to implement this primarily for simplicity. This choice leads to a slightly lower "effective thermal conductivity" for regions (of thickness less than 2δ) near a crack surface, or near a boundary surface. Note, however, that an argument can be made for this simpler approach since in most materials oxide layers form on the surface and such layers tend to have lower thermal conductivity.

In summary, in computing the temperature or the heat flux in our peridynamic model we simply do not include contributions from the t-bonds that are cut by an insulated crack (see Fig. 6).

4. Numerical convergence studies

We test the peridynamic formulation for heat conduction in Section 2.2 on two examples of heat flow in 2D domains. The first example has Dirichlet boundary conditions, while the second has Dirichlet and Neumann boundary conditions. The convergence tests in the limit of the horizon going to zero are performed by comparing the numerical peridynamic solutions with the solutions of the classical, local, model obtained analytically. Analytical solutions for the nonlocal model are not available.

4.1. Example 1: Heat transfer with Dirichlet boundary conditions

A square plate, $L = 1$ cm and $W = 1$ cm, has an initial temperature 40 °C and all boundaries are maintained at 0 °C at all times (see Fig. 8). The thermal diffusion coefficient $\alpha$is 1.14 cm^2/s ($\kappa = 1.14$ W/cm K, $\rho = 1$ kg/cm^3, and $c = 1$ J/kg K).

4.1.1. The classical model and its analytical solution

The classical formulation for the problem above is:

$$\frac{1}{\alpha}\frac{\partial\theta(\boldsymbol{x},t)}{\partial t} = \frac{\partial^2\theta(\boldsymbol{x},t)}{\partial x^2} + \frac{\partial^2\theta(\boldsymbol{x},t)}{\partial y^2}, \quad 0 < x < L, \quad 0 < y < W, \quad 0 \leqslant t < \infty$$
$$\theta(0,y,t) = \theta(L,y,t) = 0, \quad 0 \leqslant t < \infty$$
$$\theta(x,0,t) = \theta(x,W,t) = 0, \quad 0 \leqslant t < \infty$$
$$\theta(x,y,0) = 40, \quad 0 < x < L, \quad 0 < y < W$$

The analytical solution obtained with the method of separation of variables can be written as [28]:

$$\theta(x,y,t) = \sum_{m=1}^{\infty}\sum_{n=1}^{\infty} A_{mn} e^{-\alpha\left[\left(\frac{m\pi}{L}\right)^2+\left(\frac{n\pi}{W}\right)^2\right]t} \sin\frac{m\pi x}{L}\sin\frac{n\pi y}{W},$$

where

$$A_{mn} = \frac{4}{LW}\int_0^W\int_0^L \theta(x,y,0)\sin\left(\frac{m\pi x}{L}\right)\sin\left(\frac{n\pi y}{W}\right)dxdy.$$

The analytical heat flux is:

$$\boldsymbol{q}(\boldsymbol{x},t) = -\kappa\sum_{m=1}^{\infty}\sum_{n=1}^{\infty} A_{mn} e^{-\alpha\left[\left(\frac{m\pi}{L}\right)^2+\left(\frac{n\pi}{W}\right)^2\right]t} \left(\frac{m\pi}{L}\cos\frac{m\pi x}{L}\sin\frac{n\pi y}{W}\boldsymbol{i} + \frac{n\pi}{W}\sin\frac{m\pi x}{L}\cos\frac{n\pi y}{W}\boldsymbol{j}\right)$$

where $\boldsymbol{i}$ and $\boldsymbol{j}$ are unit vectors in the x and y directions.

We numerically evaluate this solution and keep a sufficient number of terms in the series so that the next term in the series is less than 10^{-12} at different times and at a set of five equally spaced points along the line $y = 0.5$. This criterion leads us to consider 19, 13, 9, and 7 terms in the series for the approximations at times 0.01, 0.025, 0.05, and 0.10 s, respectively. Due to the exponentially decaying part in the solution, this numerical approximation is very close to the exact solution, and we will refer to it as the exact solution in what follows.

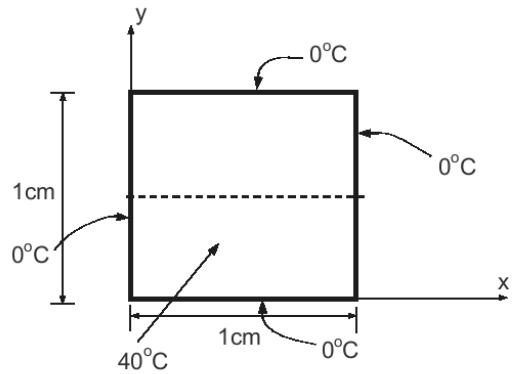

Fig. 8. Example 1: Dirichlet boundary conditions and initial temperature.

4.1.2. The computed peridynamic solution and discussion of convergence

In Fig. 9 we compare the solutions for the temperature distribution in the plate along the dotted line $y = 0.5$ in Fig. 8 obtained with the classical model and the peridynamic formulation. The peridynamic results use the conical micro-conductivity and the smallest horizon employed in this study, $\delta = \frac{13L}{480} \approx \frac{L}{40}$ and a grid spacing $\Delta x = L/256$ (which results in a value $m = \delta/\Delta x = 6.933$). The solution is plotted at various times: 0.01, 0.025, 0.05, and 0.1 s, to observe its transient nature. The horizontal heat flux at $t = 0.05$ s obtained with the same horizon and grid spacing is plotted at points along the line $y = 0.5$ in Fig. 10.

In order to observe the behavior of the nonlocal peridynamic solution relative to the solution of the classical model, we investigate the δ-convergence (see [22]). We measure the relative difference of our nonlocal solutions with respect to the classical solution by using the relative difference defined as:

$$\frac{\|\theta_{\text{classical}} - \theta_{\text{peri}}\|_2}{\|\theta_{\text{classical}}\|_2} \tag{13}$$

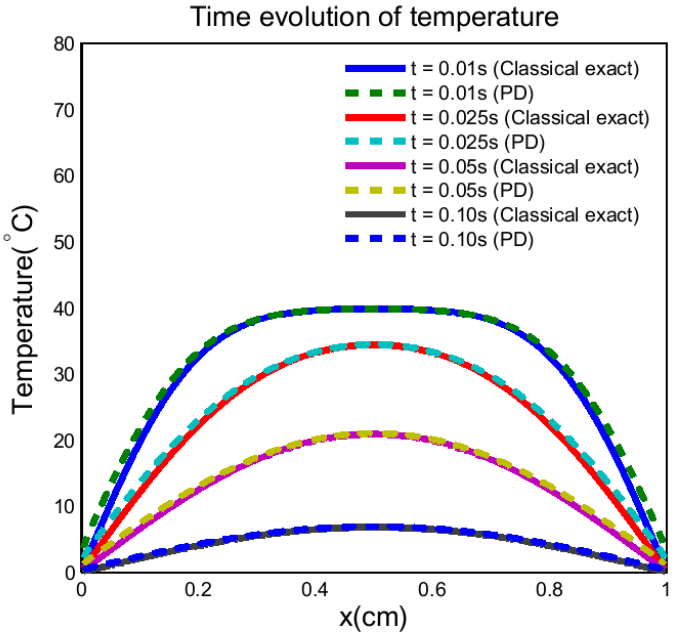

Fig. 9. Example 1: Comparison of nodal temperatures along the line $y = 0.5$ at times $t = 0.01$, 0.025, 0.05, and 0.1 s, between the classical exact solution and peridynamic solutions obtained with $\delta = 13L/480 \approx L/40$, $\Delta x = L/256$, $m = 6.933$.

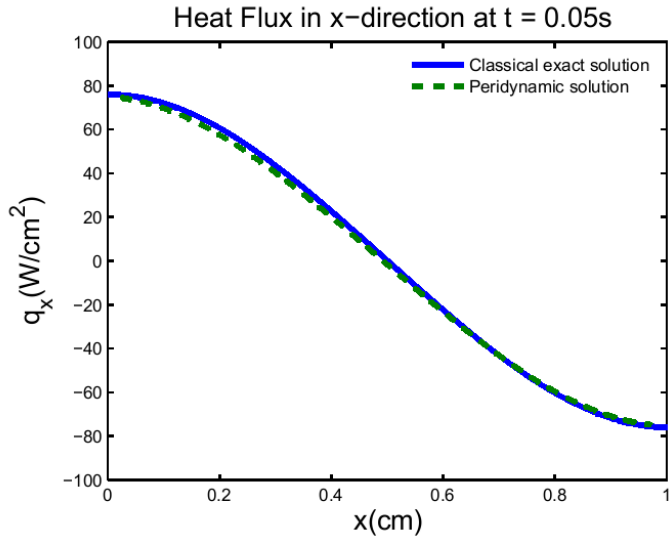

Fig. 10. Example 1: Comparison of the horizontal heat flux along the line $y = 0.5$ between classical exact solution and the peridynamic solution at time $t = 0.05$ s ($\delta = 13L/480 \approx L/40$, $\Delta x = L/256$, $m = 6.933$).

where θ_{peri} is the vector with nodal temperature values from the peridynamic numerical solution and $\theta_{classical}$ contains the exact temperature values from the classical model at the same locations (nodes) as those used in the peridynamic discrete solution. Here $\|\cdot\|_2$ is the discrete L_2 norm, or the norm-2 (the Euclidean norm) for vectors. Since we use the classical exact solution instead of the exact peridynamic solution (which is difficult to obtain), we call this measure a relative difference and not a relative error.

Convergence study: δ-convergence. In δ-convergence one takes the horizon $\delta \to 0$ while keeping $m = \delta/\Delta x$ fixed (or increasing m with decreasing δ, but at a slower rate than that of δ [22]).In the limit of the horizon going to zero the peridynamic solution converges, for problems without singularities, to the classical one.

The relative differences at $t = 0.025$ s between the temperature values from the peridynamic numerical solution and the classical exact solution along the $y = 0.5$ line for Example 1 are shown in Fig. 11 for different values of m and δ. The fact that the difference from the classical solution is less for some lower values of m than for some higher values (for a fixed horizon size) reflects the fact that the exact nonlocal solution (reachable as m tends to infinity) is different from the classical one, but the approximate solutions may start below the classical solution and pass through the classical value as m increases and we approach the exact nonlocal solution for a certain horizon size. In the 1D case, this phenomenon is described in [8] where the m-convergence curves for the solution at a point and a time instant, for various horizon sizes, intersect all at one point, a point which is also the classical exact solution. In other words, the classical exact solution could be obtained not only by taking the horizon size to zero in the nonlocal model, but also by finding the intersection point (if it exists, see [8] for an example when the curves do not intersect) of two m-convergence curves for two arbitrary horizon sizes. In 2D, the spatial integration domain (disk of radius δ) is approximated by the Algorithm 1 (see above) and the approximation error is the probable cause for which the intersection of m-convergence curves seen in 1D cases does not happen. Nevertheless, once the discretization is sufficiently fine (m is sufficiently large) the trends seen in 1D are observed in the 2D cases as well. A detailed discussion on which horizon size and number of nodes inside it to use in particular cases is provided in [29].

For values of $m > 5$ we observe that as δ goes to zero the relative difference goes to zero and the convergence is linear (see Fig. 12). The values of the relative difference between the numerical approximations to the nonlocal problems and the classical exact solution are not relevant here. As explained above, it may happen that the approximate nonlocal solution obtained with a large horizon size and a small m-value is closer to the local solution than a solution obtained with a smaller horizon size. Nevertheless, for a fixed m-value, the nonlocal solutions tend towards the classical solution as the horizon size decreases. The δ-convergence rates obviously depend on the numerical approximations used. We note that in the one-dimensional case (see [8]) where the spatial representation is exact, convergence of the primary (temperature) field is close to quadratic. With a more accurate spatial numerical integration scheme we expect quadratic rates of δ-convergence to the classical solution in 2D and 3D as well. The effect of the numerical approximation is more visible when m is small ($m < 5$) and δ-convergence does not take place. The reason is that the discretization is too coarse and the integration error from approximating the horizon region is significant. Because of this, the effective conductivity modeled may be slightly different from the one intended, and, as the horizon goes to zero one cannot guarantee convergence to the corresponding classical solution.

For $m > 5$, the m-convergence curves look similar to those obtained in the 1D case (see [8]). Since the numerical approximation of the spatial integration domain at a node (the horizon) in 2D is not exact, and for small values of m the error introduced is rather significant, the m-convergence curves do not self-intersect at the classical solution, as they did in the 1D case.

Notice that as the horizon decreases, the relative difference tends to decrease too and the nonlocal solution eventually converges to the classical solution in the limit of $\delta \to 0$ and $m \to \infty$. The data in Fig. 11 suggests we select the value

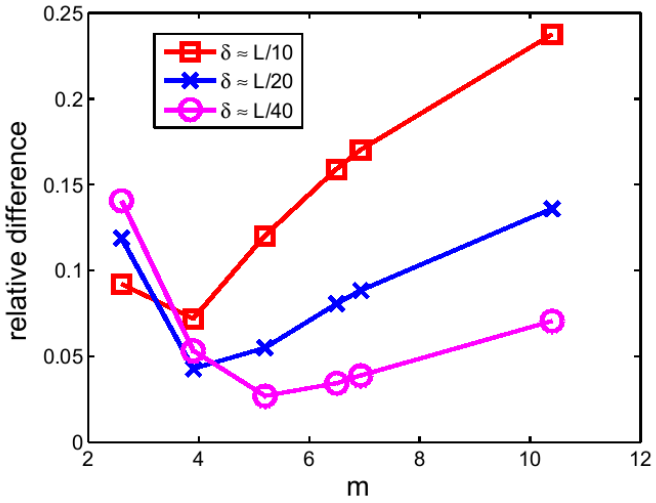

Fig. 11. Example 1: The m-convergence curves for the relative differences in temperature along the line $y = 0.5$ between the classical (local) model and the peridynamic numerical solutions (see Eq. (13)) with different horizons and number of nodes inside the horizon (different m-values).

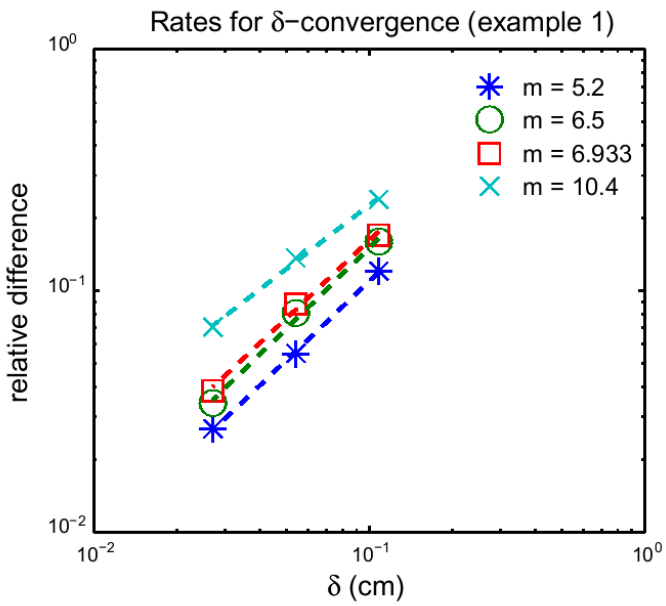

Fig. 12. Example 1: Linear rates of δ-convergence are observed for the relative difference between temperatures from the classical exact solution and the peridynamic numerical solution along $y = 0.5$ line and at time $t = 0.025$ s, when m is larger than about 5. The rates are 1.087, 1.112, 1.072, and 0.878, for $m = 5.2$, 6.5, 6.933, and 10.4, respectively.

$m = 6.5$ for all subsequent computations since it leads to more efficient computations than using larger m values and is sufficiently large so that the spatial quadrature is sufficiently accurate for a sufficiently small horizon size.

4.2. Example 2: Heat transfer with Neumann and Dirichlet boundary conditions

The square plate, $L = 1$ cm and $W = 1$ cm, now has a temperature boundary condition, $\theta = 1$ °C, on the left boundary and zero heat flux imposed on the remaining boundaries (see Fig. 13). An initial temperature of 0 °C is prescribed. We choose a thermal diffusion coefficient $\alpha = 1$ cm^2/s, $\kappa = 1$ W/cm K, $\rho = 1$ kg/cm^3, and $c = 1$ J/kg K.

4.2.1. The classical formulation and its analytical solution

The classical formulation, in non-dimensional form, is:

$$\frac{\partial\theta(\boldsymbol{x},t)}{\partial t} = \frac{\partial^2\theta(\boldsymbol{x},t)}{\partial x^2} + \frac{\partial^2\theta(\boldsymbol{x},t)}{\partial y^2}, \quad 0 < x < 1, \quad 0 < y < 1, \quad 0 \leqslant t < \infty \tag{14}$$

$$\theta_y(x,0,t) = \theta_y(x,1,t) = 0, \quad 0 \leqslant t < \infty \tag{15}$$

$$\theta(0,y,t) = 1, \quad \theta_x(1,y,t) = 0, \quad 0 \leqslant t < \infty \tag{16}$$

$$\theta(x,y,0) = 0, \quad 0 < x < 1, 0 < y < 1 \tag{17}$$

The analytical solution, using the method of separation of variables, along the line $y = 0.5$ is given by [30]:

$$\theta(x, y = 0.5, t) = 1 + \sum_{n=1}^{\infty} \tilde{b}_{0n} e^{-(\beta_n^2)t} \sin \beta_n x \tag{18}$$

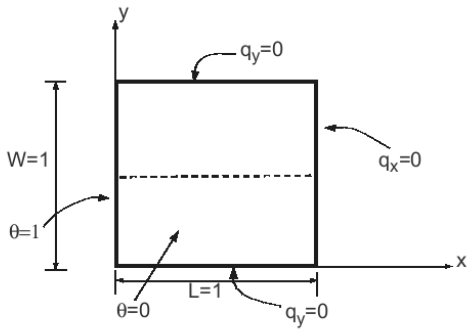

Fig. 13. Example 2: Problem setup.

and the analytical heat flux is:

$$q(x, y = 0.5, t) = -\kappa \sum_{n=1}^{\infty} \tilde{b}_{0n} e^{-(\beta_n^2)t} \frac{\cos \beta_n x}{\beta_n} \tag{19}$$

where

$$\tilde{b}_{0n} = \frac{\cos \beta_n - 1}{\left(1/2 - \frac{\sin(2\beta_n)}{4\beta_n}\right)\beta_n},$$

and

$$\beta_n = \frac{(2n-1)\pi}{2}.$$

We numerically evaluate this solution and keep a sufficient number of terms in the series so that the next term in the series is less than 10^{-12} at different times and at a set of five equally spaced points along the line $y = 0.5$. This criterion leads us to consider 9, 7 and 6 terms in the series for the approximations at times 0.05, 0.10, and 0.20 s, respectively. Due to the exponentially decaying part in the solution, this numerical approximation is very close to the exact solution, and we will refer to it as the exact solution in what follows.

4.2.2. The peridynamic solution and discussion of convergence

We compute the peridynamic temperatures along the dotted line $y = 0.5$ in Fig. 13 and test δ-convergence for $m = 6.5$. We use three different horizon sizes $\delta = 13L/120$, $13L/240$, $13L/480$ (which, for the m chosen leads to total number of nodes of 61×61, 121×121, 241×241, respectively).

For the smallest two horizon values, the peridynamic solutions are compared, at different times, with the classical exact solution in Fig. 14. The relative differences in the temperature values computed using Eq. (13) are seen in Table 1 for the three horizon sizes and at different times. The plots in Fig. 15 show the rates of δ-convergence for $m = 6.5$ and at times $t = 0.05$, 0.1, and 0.2 s. The rates are linear (1.09, 1.15, and 1.0, for the three horizon sizes, respectively).

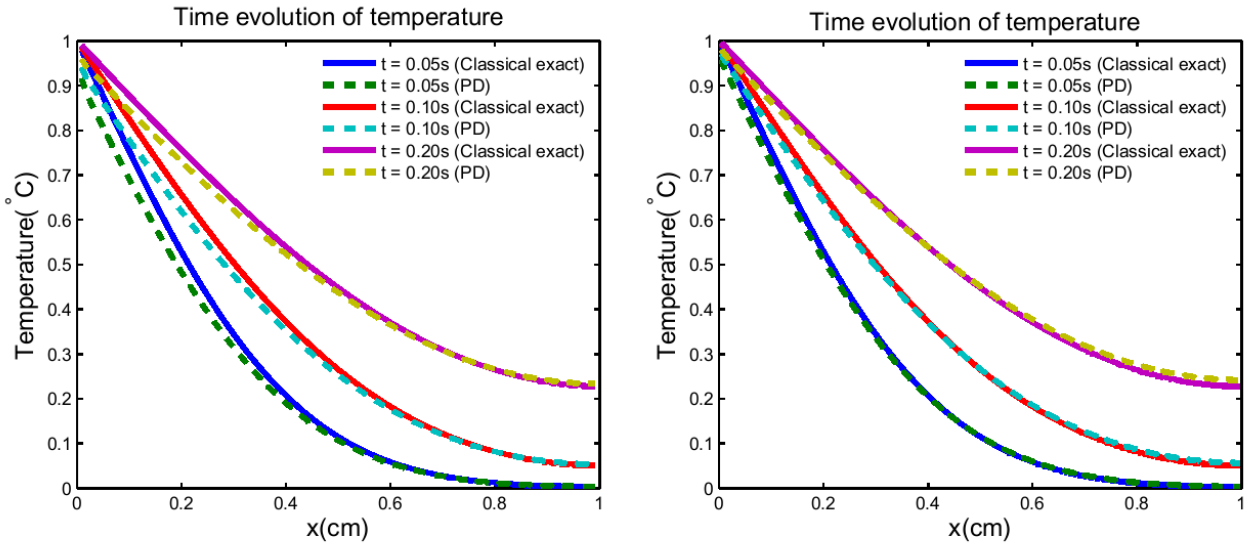

Fig. 14. Example 2: Comparison of temperatures along the line $y = 0.5$ between the classical exact solution and the peridynamic solution at times $t = 0.05$, 0.1, and 0.2, for $\delta = 13L/240$ (left) and $\delta = 13L/480$ (right). $m = 6.5$ in both cases.

Table 1
Example 2: Relative differences in temperatures (see Eq. (13) along the line $y = 0.5$ between the classical model and peridynamic solutions with different horizons and $m = 6.5$ for different times.

t(s)	$\delta = \frac{13L}{120} \approx \frac{L}{10}$	$\delta = \frac{13L}{240} \approx \frac{L}{20}$	$\delta = \frac{13L}{480} \approx \frac{L}{40}$
0.05	0.15741	0.07927	0.03474
0.1	0.11342	0.05301	0.02302
0.2	0.07517	0.03203	0.01881

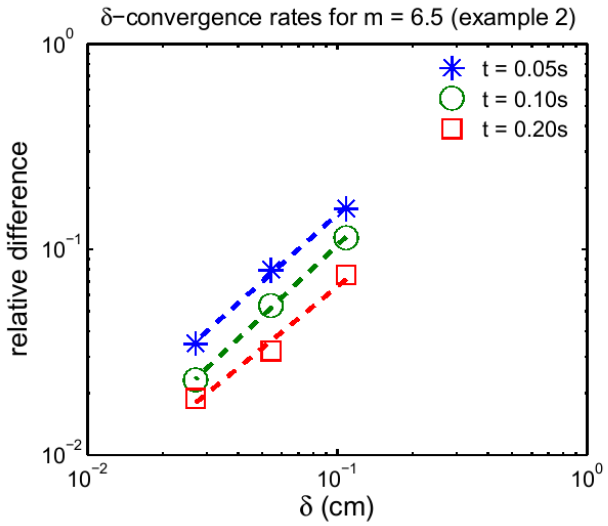

Fig. 15. Example 2: The δ-convergence rates for the relative difference between the classical exact solution and the peridynamic numerical solutions along $y = 0.5$ line, at three different times and for $m = 6.5$.

5. Heat flow over insulated stationary or growing cracks, and in thermally heterogeneous systems

In this section we analyze heat flow over insulated cracks and in composite materials. For the case of stationary and non-intersecting cracks we compare the peridynamic results with those from an ABAQUS finite element solution, or with solutions published in the literature. We also consider a case of transient heat transfer in a plate in which two insulating cracks are growing and crossing each other. The damage model introduced in Section 2.4 and the discussions in Sections 3.4 and 3.5 are used here. Finally, we model transient heat flow in a thermally heterogenous system, similar to a fiber-reinforced composite. Thermal bonds that connect nodes in material regions that have different conductivity values are matched to the material with a lower conductivity (see [31]).

5.1. Example 3: Heat flow in a plate with an insulated crack

To verify the damage model for thermal bonds we solve the problem of heat flow in a plate with an insulated crack with both the peridynamic approach and with ABAQUS that uses a finite element discretization of the classical model.

Consider a square plate, $L = 2$ cm and $W = 2$ cm, with a single insulated horizontal crack of length $2a$ ($a = 0.5$ cm), centered at the origin, and an initial temperature 0 °C. The left and right boundaries are insulated. Temperatures of ±100 °C are imposed on the top and bottom boundaries, respectively (see Fig. 16) at all times. The thermal diffusion is 1.14 cm^2/s. The solution (temperature values) given by ABAQUS using 1620 linear quadrilateral elements at $t = 0.5$ s (in the steady-state regime) is shown in Fig. 17. For the peridynamic solutions we use $m = 6.5$, and two different horizons: $\delta = 13L/240$ and $13L/480$. The peridynamic results at $t = 0.5$ s in Fig. 18 are very close to the classical solution obtained in Fig. 17.

5.2. Example 4: Heat transfer in a plate with multiple insulated cracks

For the case of heat flow over multiple insulated cracks we refer to the solutions provided in [3] using the finite element alternating method and in [7] using the alternating method. We consider the same setup as the ones used in [3,7]: heat flow

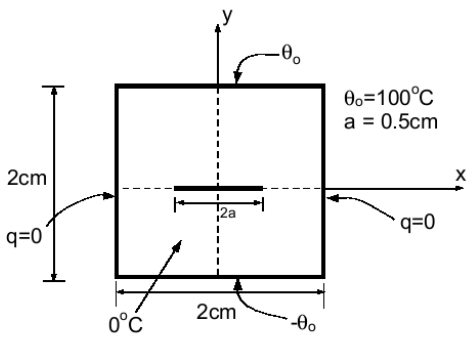

Fig. 16. Example 3: Problem description for heat flow in a plate with an insulating crack.

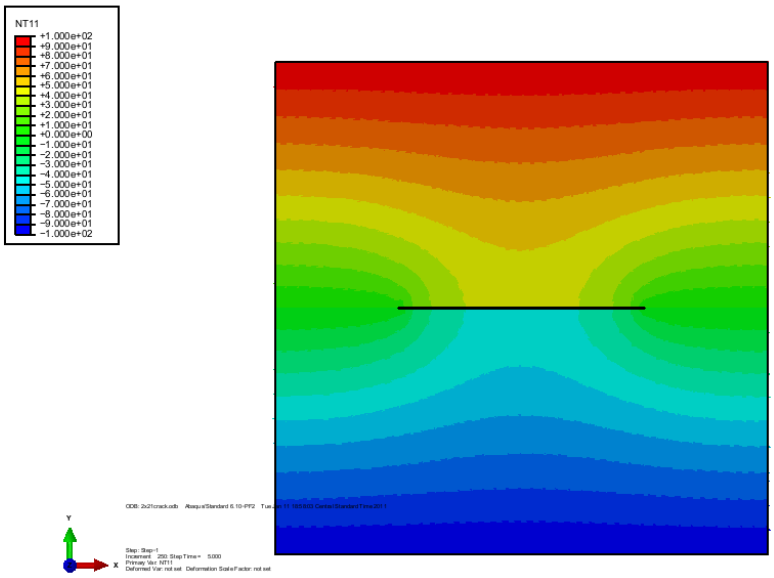

Fig. 17. Example 3: The temperature distribution at time $t = 0.5$ s for the classical model using an ABAQUS finite element discretization with 1620 linear quadrilateral elements.

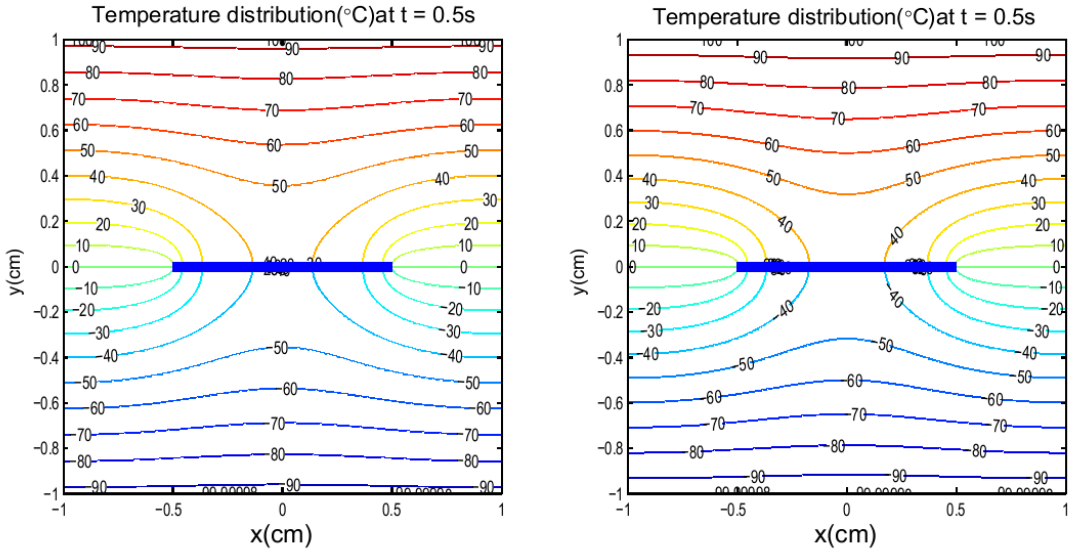

Fig. 18. Example 3: The temperature distribution at time $t = 0.5$ s obtained with peridynamics using $m = 6.5$, and $\delta = 13L/240$ (left) and $\delta = 13L/480$ (right).

in a square plate ($L = 2$ cm, $W = 2$ cm) with two inclined insulated cracks as shown in Fig. 19(left). The initial temperature is 0 °C. The left and right boundaries are insulated. Temperatures of ±100 °C are imposed on the top and bottom boundaries, respectively. Thermal diffusion is 1.14 cm^2/s.

The plots in Fig. 20 show the peridynamic solution. We run the test until $t = 4.5$ s to ensure that it reaches steady state conditions so that we can compare with the results for the classical model given in [7,3]. We employ $\delta = 13L/120$ and $13L/240$, and $m = 6.5$. The isotherms from the peridynamic results shown in Fig. 20 are similar to those shown in Fig 19(right) which are reproduced from [7,3]. The results obtained with the smaller horizon are, as expected, closer to those from the classical model.

5.3. Example 5: Heat flow over insulated growing and intersecting cracks

The problem of heat flow over growing, interacting cracks has received little attention in the classical treatment. In general, problems in which discontinuities in the unknown field are suddenly generated, and evolve and interact in time, are not easy to consider with a classical treatment because of complications related to the mathematical representation of derivatives over discontinuities. Peridynamics eliminates these difficulties since spatial derivatives do not appear in the

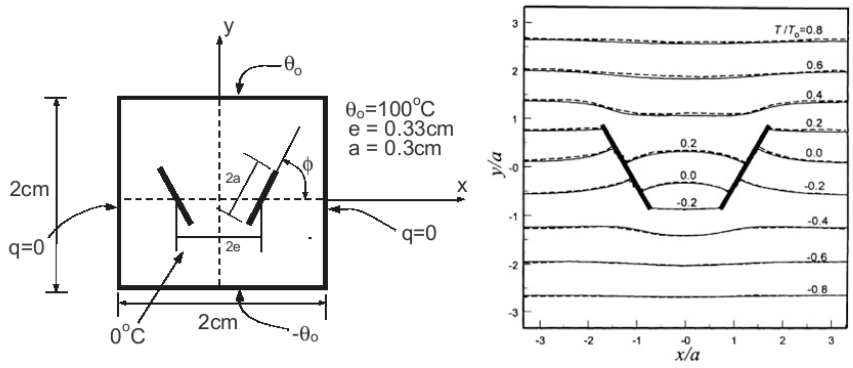

Fig. 19. Example 4: Problem settings (left) and temperature distribution (right) from the classical model obtained in [7] (solid lines) and [3] (dash lines). The inclination angle is $\phi = \pi/3$.

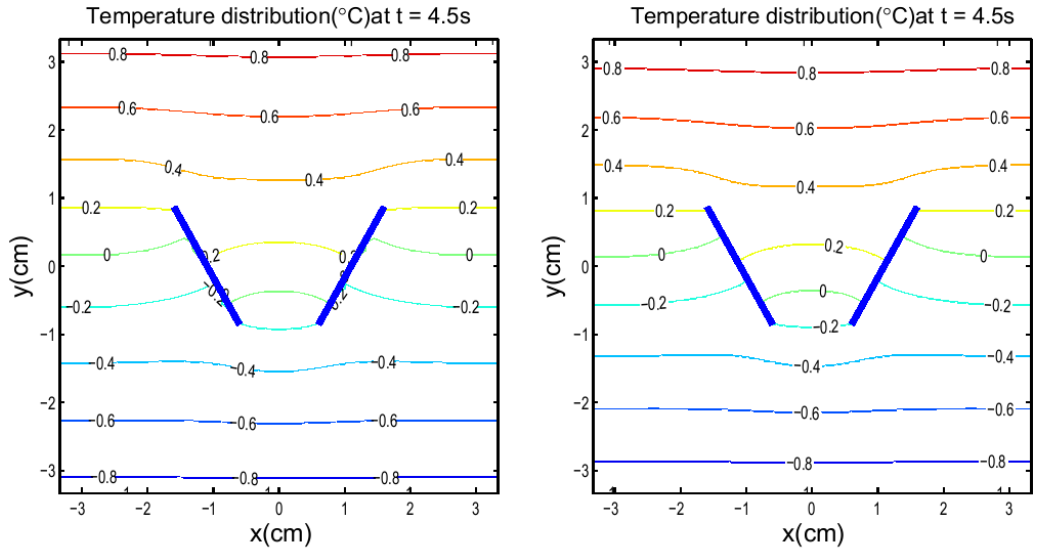

Fig. 20. Example 4: Contour plots of peridynamic temperatures at $t = 4.5$ s obtained for $m = 6.5$, $\delta = 13L/120$ (left) and $13L/240$ (right).

formulation. To demonstrate this advantage we consider the problem of transient heat flow in a plate in which two insulating cracks form, grow, and intersect. The growth of these cracks is imposed by us here. We simply cut the thermal bonds that cross certain growing segments to model the formation of insulating cracks (see Sections 2.4, 3.4, and 3.5). In a future thermomechanical peridynamic model the dynamic cracks will be part of the solution, being induced by the thermomechanical loadings.

We consider a square plate ($L = 2$ cm and $W = 2$ cm) with two growing cracks, which start at points (x_1,y_1) and (x_2,y_2) and move diagonally across the plate, as shown in Fig. 21. The two cracks start to grow at time $t = 0$ with a constant velocity

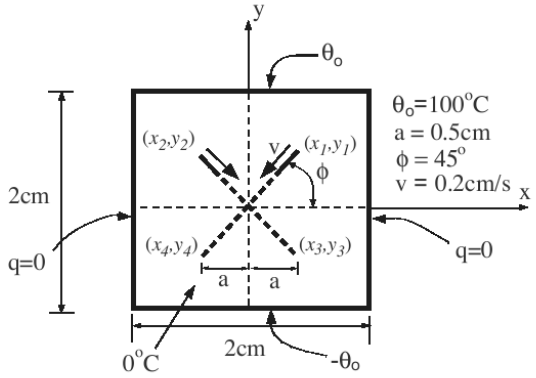

Fig. 21. Example 5: Problem setup for the heat flow problem in a plate with growing and intersecting insulated cracks.

0.2 cm/s chosen so that at the end of the simulation a symmetric $\times$-like crack is obtained. The initial temperature in the plate is 0 °C. The left and right boundaries are insulated and temperatures of ±100 °C are imposed on the top and bottom

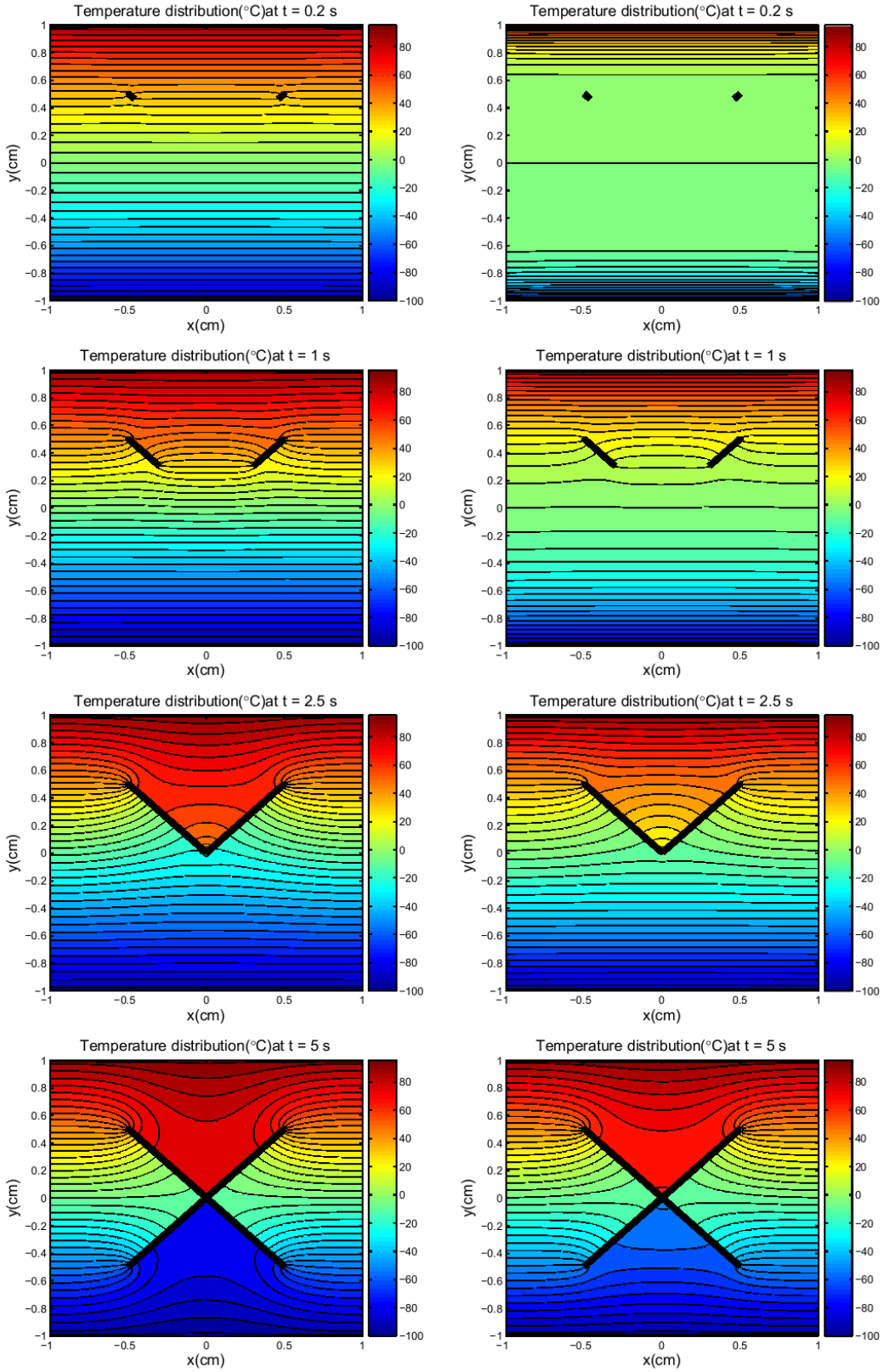

Fig. 22. Example 5: Contour plots for the evolution of peridynamic temperature. The thermal diffusion is larger (1.14 cm^2/s) for results in the left column, and is 0.114 cm^2/s for results in the right column.

boundaries, respectively (see Fig. 21). We solve two cases: a higher thermal diffusivity of 1.14 cm^2/s, and a lower one of 0.114 cm^2/s. We use the same horizon $\delta = 13L/240$ and the same $m = 6.5$.

The solutions are shown in Fig. 22. In the higher conductivity case, the steady-state solution for a plate without cracks is reached before the cracks grow much. As the cracks grow and close down the gap between them, the temperature rises in the V area and drops below it. The temperature values near the center of the plate, just above and below of the intersecting point of the two cracks, jump from one another once the cracks intersect and continue to grow. The shielding effect induced by connecting the insulating cracks is correctly captured by the peridynamic solution.

5.4. Example 6: Transient heat flow in a fiber-reinforced composite

To demonstrate the ability of the proposed peridynamic model in solving problems set in thermally heterogeneous materials we consider the transient heat-flow problem in a periodic cell of the microstructure in a hypothetical fiber-reinforced

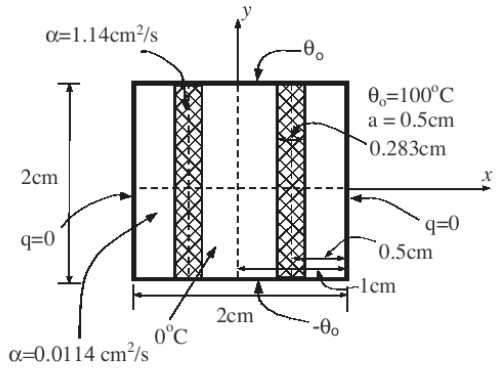

Fig. 23. Example 6: The problem setup for heat flow in a thermally heterogeneous material.

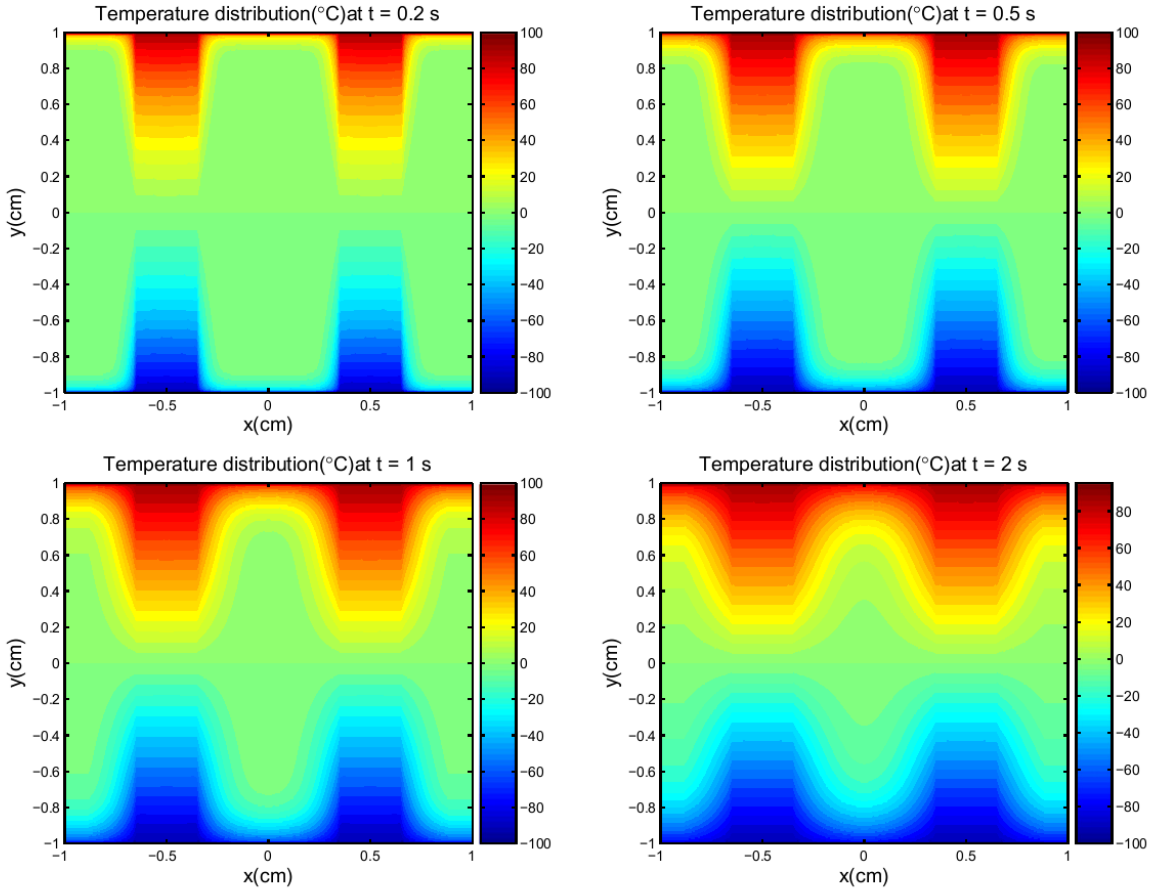

Fig. 24. Example 6: Time-evolution (from 0.2 to 2 s) of the temperature field ($m = 6.5$, $\delta = 13L/240$).

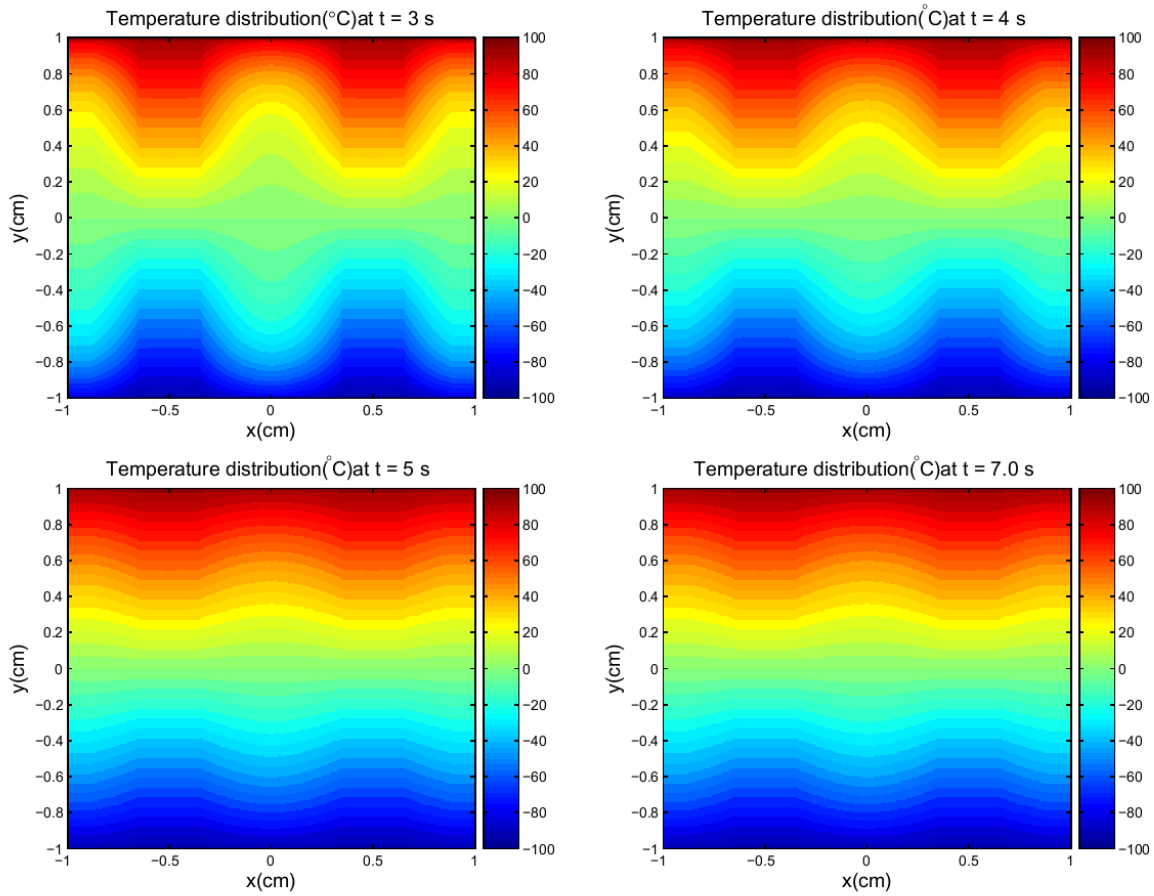

Fig. 25. Example 6: Time-evolution (from 3 to 7 s) of the temperature field ($m = 6.5$, $\delta = 13L/240$).

composite (FRC) material. Here we explicitly model the material microstructure. Homogenization approaches can be developed. For homogenization in the mechanical model of peridynamics for FRCs see, for example, [32,20].

We consider a sample cut from a the continuous fiber-reinforced composite as shown in Fig. 23. The initial temperature is 0 °C and the left and right boundaries are insulated to simulate periodic boundary conditions. We impose temperatures of ± 100 °C on the top and bottom boundaries, respectively. The two "fiber inclusions" have a thermal diffusivity of 1.14 cm^2/s, while the "matrix" has a diffusivity 100 times smaller: 0.014 cm^2/s (see Fig. 23). We solve the problem using a horizon size $\delta = 13L/240$ and $m = 6.5$.

Note that in the case of a thermally heterogenous material, one has to assign special microconductivity values for t-bonds that connect nodes from regions with different conductivities. In such instances, we have observed (see [31]) that choosing the microconductivity corresponding to the material with the lower conductivity works well in modeling peridynamic heat transfer in a composite bar. We use the same strategy here.

Figs. 24 and 25 show the heat flow in the body at different times. Temperatures rise faster in the high diffusivity material (the "fibers"), as the heat "deflects" from the low conductivity regions to flow through the high conductivity regions. The model goes into steady-state at about 5 s. The steady-state approaches, but does not coincide with the solution for a homogeneous material in which the isotherms are horizontal lines. Notice the sharp thermal gradients near the interfaces between the "fibers" and the "matrix" material, especially at the early times. Such steep thermal gradients induce differences in the thermal expansion of the component materials and can lead to delamination between the fibers and the matrix in a FRC under thermal fatigue. Reports in the literature indicate (see e.g., [33,34]) that intra and interlaminar cracks due to thermal fatigue can form significantly sooner than when the composite is subjected to purely mechanical fatigue.

6. Conclusion and future work

We introduced a peridynamic formulation for modeling transient heat transfer in multi-dimensional domains. The formulation, which does not contain spatial derivatives of the temperature field, is suitable for modeling heat transfer in bodies with complexly evolving discontinuities such as growing cracks that interact in any arbitrary way. We introduced the peridynamic heat flux to match the classical heat flux for problems in which the temperature profile is linear. In general, the peridynamic heat flux converges to the classical heat flux in the limit of the nonlocal region (the horizon) going to zero.

The peridynamic heat flux is more general than the classical one and it exists even when isotherms are not smooth surfaces, or at corners of the domain.

We showed that the results from the peridynamic model for heat flow problems in 2D converge to the analytical solutions of the corresponding classical (local) models, in the limit of the peridynamic horizon going to zero, while the number of nodes inside the horizon is kept constant. This convergence does not preclude the situation in which the numerical approximation of the nonlocal model obtained with a larger horizon and a small number of nodes inside the horizon is closer to the classical result than an approximation obtained with a smaller horizon and a larger number of nodes inside the horizon. We employed the peridynamic formulation for solving transient heat conduction problems in bodies with discontinuities such as insulated cracks. For static, nonintersecting cracks we verified the formulation of damage in thermal peridynamic bonds against finite element solutions. The new model allowed us to solve, without extra difficulties, heat flow problems in a body in which insulated cracks dynamically grow, intersect, and thus alter the heat flow patterns. We also solved a problem of heat transfer in a thermally heterogeneous material, like a fiber-reinforced composite. The particular heat flow along the fiber direction induced by temperature differences between the boundaries and the interior led to the formation of steep thermal gradients at the fiber/matrix interface. Such thermal gradients can determine premature failure of the composite via intralaminar delamination (splitting failure at the fiber/matrix interface).

The formulation can be used in the future to, for example, evaluate effective thermal (or even electroelastic) conductivities in materials with an arbitrary distribution of insulating or permeable, possibly intersecting cracks of arbitrary shapes. Some analytical solutions exist for the case with straight non-intersecting cracks (see [35]).

Coupling between the mechanical and thermal peridynamic models are planned for the future.

Acknowledgements

This work has been supported, in part, by the Sandia National Laboratories, Albuquerque, NM (Contract Number 568428, project coordinator Dr. S.A. Silling) and by ARL, Aberdeen Proving Grounds, MD (ARO Proposal Number 58450-EG, Project Managers Dr. Chian-Fong Yen and Dr. Charles Randow). We wish to extend special thanks to Dr. S.A. Silling, Dr. R.B. Lehoucq, and Dr. M.L. Parks of Sandia, for stimulating discussions.

References

[1] G.C. Sih, Heat conduction in the infinite medium with lines of discontinuities, Journal of Heat Transfer 87 (1965) 293–298.
[2] T.L. Anderson, Fracture Mechanics: Fundamentals and Applications, third ed., CRC Press, Florida, 2005.
[3] W.H. Chen, C.L. Chang, Heat conduction analysis of a plate with multiple insulated cracks by the finite element alternating method, International Journal of Solids and Structures 31 (10) (1994) 1343–1355.
[4] W.H. Chen, C.S. Chang, Analysis of two-dimensional mixed mode crack problems by finite element alternating method, Computers and Structures 33 (1989) 1451–1458.
[5] W.H. Chen, C.S. Chang, Analysis of two-dimensional fracture problems with multiple cracks under mixed boundary condition, Engineering Fracture Mechanics 34 (1989) 921–934.
[6] L.V. Kantorovich, V.I. Krylov, Approximate Methods of Higher Analysis, Interscience, 1964.
[7] C.Y. Chang, C.C. Ma, Transient thermal conduction analysis of a rectangular plate with multiple insulated cracks by the alternating method, International Journal of Heat and Mass Transfer 44 (13) (2001) 2423–2437.
[8] F. Bobaru, M. Duangpanya, The peridynamic formulation for transient heat conduction, International Journal of Heat and Mass Transfer 53 (19-20) (2010) 4047–4059.
[9] M. Dubé, V. Doquet, A. Constantinescu, D. George, Y. Rémond, S. Ahzi, Modeling of thermal shock-induced damage in a borosilicate glass, Mechanics of Materials 42 (9) (2010) 863–872.
[10] N. Joulaee, A. Makradi, S. Ahzi, M.A. Khaleel, B.K. Koeppel, Prediction of crack propagation paths in the unit cell of SOFC stacks, International Journal of Mechanics and Materials in Design 5 (2009) 217–230.
[11] S. Nemat-Nasser, L.M. Keer, K.S. Parihar, Unstable growth of thermally induced interacting cracks in brittle solids, International Journal of Solids and Structures 14 (6) (1978) 409–430.
[12] D.R. Jenkins, Determination of crack spacing and penetration due to shrinkage of a solidifying layer, International Journal of Solids and Structures 46 (5) (2009) 1078–1084.
[13] L. Niemeyer, L. Pietronero, H. Wiesmann, Fractal dimension of dielectric breakdown, Physical Review Letters 52 (12) (1984) 1033–1036.
[14] H.R. Zeller, Breakdown and prebreakdown in solid dielectrics, IEEE Transactions on Electrical Insulation 22 (2) (1987) 115–122.
[15] I.V. Lisitsyn, H. Inoue, I. Nishizawa, S. Katsuki, H. Akiyama, Breakdown and destruction of heterogeneous solid dielectrics by high voltage pulses, Journal of Applied Physics 84 (11) (1998) 6262–6267.
[16] O.I. Craciunescu, S.K. Das, R.L. Mccauley, J.R. Macfall, T.V. Samulski, 3D numerical reconstruction of the hyperthermia induced temperature distribution in human sarcomas using DE-MRI measured tissue perfusion: validation against non-invasive MR temperature measurements, International Journal of Hyperthermia 17 (3) (2001) 221–239.
[17] E.L. Jones, J.R. Oleson, L.R. Prosnitz, T.V. Samulski, Z. Vujaskovic, D.H. Yu, L.L. Sanders, M.W. Dewhirst, Randomized trial of hyperthermia and radiation for superficial tumors, Journal of Clinical Oncology 23 (13) (2005) 3079–3085.
[18] B.E. Dayanc, S.H. Beachy, J.R. Ostberg, E.A. Repasky, Dissecting the role of hyperthermia in natural killer cell mediated anti-tumor responses, International Journal of Hyperthermia 24 (1) (2008) 41–56.
[19] C. Kim, A.P. O'Rourke, J.A. Will, D.M. Mahvi, J.G. Webster, Finite-element analysis of hepatic cryoablation around a large blood vessel, IEEE Transactions on Biomedical Engineering 55 (8) (2008) 2087–2093.
[20] W. Hu, Y.D. Ha, F. Bobaru, Peridynamic model for dynamic fracture in unidirectional fiber-reinforced composites, Computer Methods in Applied Mechanics and Engineering (2012), accepted for publication.
[21] Y.T. Feng, K. Han, C.F. Li, D.R.J. Owen, Discrete thermal element modelling of heat conduction in particle systems: basic formulations, Journal of Computational Physics 227 (10) (2008) 5072–5089.
[22] F. Bobaru, M. Yang, L.F. Alves, S.A. Silling, E. Askari, J. Xu, Convergence, adaptive refinement, and scaling in 1d peridynamics, International Journal for Numerical Methods in Engineering 77 (6) (2009) 852–877.
[23] Y.D. Ha, F. Bobaru, Studies of dynamic crack propagation and crack branching with peridynamics, International Journal of Fracture 162 (1–2) (2010) 229–244.

[24] S.A. Silling, E. Askari, A meshfree method based on the peridynamic model of solid mechanics, Computers and Structures 83 (17–18) (2005) 1526–1535.
[25] Y.D. Ha, F. Bobaru, Characteristics of dynamic brittle fracture captured with peridynamics, Engineering Fracture Mechanics 78 (6) (2011) 1156–1168.
[26] S.A. Silling, Reformulation of elasticity theory for discontinuities and long-range forces, Journal of the Mechanics and Physics of Solids 48 (2000) 175–209.
[27] W. Hu, Y.D. Ha, F. Bobaru, Numerical integration in peridynamics, Technical report, Department of Engineering Mechanics, University of Nebraska-Lincoln, 2010.
[28] R.P. Agarwal, D. O'Regan, Ordinary and Partial Differential Equations, Springer, New York, 2009.
[29] F. Bobaru, The meaning, selection, and use of the peridynamic horizon, International Journal of Fracture, in press.
[30] H.M. Srivastava, K.Y. Kung, K.J. Wang, Analytic solutions of a two-dimensional rectangular heat equation, Russian Journal of Mathematical Physics 14 (1) (2007) 115–119.
[31] M. Duangpanya. A peridynamic formulation for transient heat conduction in bodies with evolving discontinuities, Ph.D. Thesis, University of Nebraska-Lincoln, Lincoln, Nebraska, March 2011.
[32] W. Hu, Y.D. Ha, F. Bobaru, International Journal for Multiscale Computational Engineering, Modeling dynamic fracture and damage in fiber-reinforced composites with peridynamics 9 (6) (2011) 707–726.
[33] D. Leveque, A. Schieffer, A. Mavel, J.F. Maire, Analysis of how thermal aging affects the long-term mechanical behavior and strength of polymer-matrix composites, Composites Science and Technology 65 (3-4) (2005) 395–401.
[34] K. Giannadakis, J. Varna, Effect of thermal aging and fatigue on failure resistance of aerospace composite materials, in: D. Horwat, T. Czerwiec, Z. Ayadi, B. Jamart, (Eds.), 5th International EEIGM–AMASE–FORGEMAT Conference on Advanced Materials Research, IOP Conference Series – Materials Science and Engineering, 2009.
[35] X. Wang, G. Gazonas, M. Santare, On the effective electroelastic properties of microcracked generally anisotropic solids, International Journal of Fracture 158 (2009) 27–40.